

## CHAPTER 4: THE ROLE OF EPIDERMAL ABSORPTION COEFFICIENTS APPLICABLE TO THE SOUTH AFRICAN POPULATION

As mentioned previously, the quality of any computer model is determined by the applicability of the assumptions and the accuracy of the input data. In the epidermal layer, the absorption coefficient of the epidermis is an important parameter as it contributes to the reduction in fluence rate as the light propagates through the tissue. As discussed in section 2.3.2 the values of  $\mu_a$  for the epidermis are not readily available in the literature for the different skin phototypes (see Table 2.3). The South African population presents a wide variety of skin phototypes. The difference in epidermal absorption of the different skin phototypes is an important parameter in laser treatment planning.

A non-invasive diffuse reflectance optical system was developed to calculate  $\mu_a$  from actual reflectance measurements. After the system was calibrated on liquid skin simulating phantoms, 30 volunteers were recruited at the National Laser Centre (NLC, CSIR) and measurements were done according to approved ethics protocols. Ethics approval was obtained from both the CSIR (Ref 17/2011, Appendix I) and the University of Pretoria (EC110830-060, Appendix II).

### 4.1 DIFFUSE REFLECTANCE THEORY AND MODEL DEVELOPMENT

The reflectance probe calibration and data reduction methods are mainly based on the work of Zonios (Zonios G, 2006), (Zonios G, 2008(a)). In order to use the diffuse reflectance theory, a few assumptions need to be made. These are that the tissue is a homogenous, semi-infinite and turbid medium (Zonios G, 2006). Part of the light incident on the tissue surface (skin) will be absorbed (dependent on  $\mu_a$ ) while part of the non-absorbed light will be scattered multiple times and eventually exit the skin surface as diffused reflected light as illustrated in Figure 4.1 (same as Figure 2.10 in section 2.3.1.6).

The total diffuse reflection ( $R_t$ ) is given by (Zonios G, 2006):

$$R_t = \frac{\mu'_s}{\mu'_s + \mu_a} \quad (4.1)$$

$R_t \rightarrow 0$  for high absorbance skin and  $R_t \rightarrow 1$  for low absorbance skin. This derivation is acceptable on a qualitative basis, but for a more quantitative expression an empirical factor,

$k$ , is introduced to rescale  $\mu'_s$  with  $\mu'_s/k$ . Introducing this in Eq 4.1 results in the following equation:

$$R_t = \frac{1}{1 + k \frac{\mu_a}{\mu'_s}} \quad (4.2)$$

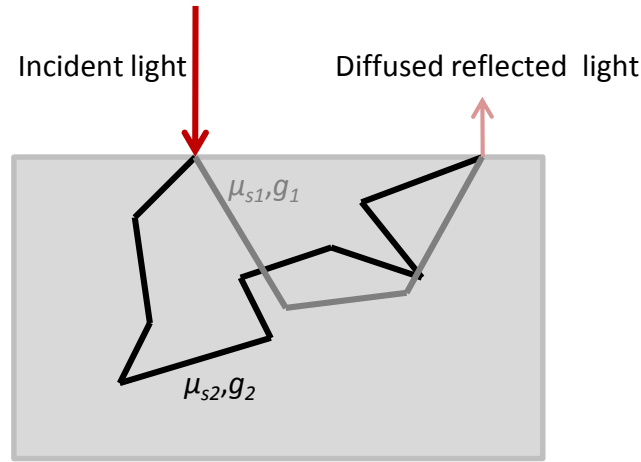


Figure 4.1: Diffuse reflected light.

Eq 4.2 is not suitable to describe diffuse reflectance measured with small diameter fibre optics. Due to the small fibre diameter (typically 200-400  $\mu\text{m}$ ), the fibre only measures part of the diffuse reflected light that emerges from the skin and breaks the inherent scale invariance in Eq 4.2. The scale invariance can be removed from Eq 4.2 by introducing an explicit dependence on  $\mu'_s$  and rewriting Eq 4.2 for the diffuse reflectance measured by the probe ( $R_p$ ) as (Zonios G, 2006):

$$R_p = \frac{1}{k_1 \frac{1}{\mu'_s} + k_2 \frac{\mu_a}{\mu'_s}} \quad (4.3)$$

where  $k_1$  and  $k_2$  are now parameters that depend on the probe geometry as well as the indices of reflection for the skin and the surrounding medium (usually air).

The major absorbing components in skin contributing to the absorption coefficient are the oxyhaemoglobin and deoxyhaemoglobin concentrations ( $c_{HbO_2}$  and  $c_{Hb}$ ), oxygen saturation ( $\alpha$ ) and melanin concentration ( $c_{mel}$ ). Water is also an absorber in skin, but in the wavelength band considered in this work (450-800 nm), the contribution of water is at least an order of magnitude smaller than that of the blood and melanin (see Figure 2.7) and is not included. The absorption of haemoglobin and melanin are wavelength dependent and contribute to the absorption coefficient through (Zonios G, 2006):

$$\mu_a(\lambda) = c_{HbO_2}[\alpha\varepsilon_{HbO_2}(\lambda) + (1 - \alpha)\varepsilon_{Hb}(\lambda)] + c_{mel}\varepsilon_{mel}(\lambda) \quad (4.4)$$

with:

$c_{HbO_2}$  = oxyhaemoglobin concentration

$c_{mel}$  = melanin concentration

$\varepsilon_{HbO_2}(\lambda)$  = extinction coefficient for oxyhaemoglobin (Prahl S, 1999)

$\varepsilon_{Hb}(\lambda)$  = extinction coefficient for deoxyhaemoglobin (Prahl S, 1999)

$\varepsilon_{mel}(\lambda)$  = extinction coefficient for melanin (Jacques SL, 1998(a))

$\alpha$  = oxygen saturation level of blood, defined as the ratio of the oxygenated

blood to the total blood concentration  $\alpha = \frac{c_{HbO_2}}{c_{HbO_2} + c_{Hb}}$

In order to model the scattering coefficient an effective scattering size ( $d_s$ ) is introduced as follows (Zonios G, 2008(a)):

$$\mu'_s(\lambda) = \left[ 1 - \left( \frac{d_0}{d_s} \right)^{1/2} \left( \frac{\lambda - \lambda_1}{\lambda_2 - \lambda_1} \right) \right] \mu'_s(\lambda_1) \quad (4.5)$$

with:

$d_0$  = constant = 0.0625  $\mu\text{m}$  (Zonios G, 2006)

$d_s$  = effective scatter size

$\lambda_1$  = min ( $\lambda$ ) = 450 nm

$\lambda_2$  = max ( $\lambda$ ) = 800 nm

The linear dependence of  $\mu'_s$  on wavelength is a reasonable approximation and is supported by the Mie theory for spherical scatterers (Zonios G, 2001). In the diffuse reflection model used for this work the particle size parameters were combined in a single parameter,  $c_d$ , that is related to the particle size. Eq 4.5 was then simplified to (Zonios G, 2008(b)):

$$\mu'_s(\lambda) = \left[ 1 - c_d \left( \frac{\lambda - \lambda_1}{\lambda_2 - \lambda_1} \right) \right] \mu'_s(\lambda_{min}) \quad (4.6)$$

with:

$c_d$  = scatter size parameter

$\lambda_1$  = min ( $\lambda$ ) = 450 nm

$\lambda_2$  = max ( $\lambda$ ) = 800 nm

The MATLAB function LSQCURVEFIT was used to solve Eq. 4.3 in a least-squares sense using nonlinear curve-fitting. The measured probe reflectance is described mathematically in terms of five coefficients ( $c_{HbO_2}$ ,  $\alpha$ ,  $c_{mel}$ ,  $c_d$ ,  $\mu'_s(\lambda_{min})$ ) that are adjusted to

best match the equation to the experimental data. The function requires an initial estimate of the parameters to be optimized and has the option to include constraints. According to the MATLAB online documentation the algorithm is a “subspace trust-region method and is based on the interior-reflective Newton method” described by Coleman (Coleman T, 1994), (Coleman T, 1996), where each iteration involves the approximate solution of a large linear system using the method of preconditioned conjugate gradients (PCG).

In Eq 4.4 provision is made for only one melanin extinction coefficient ( $\varepsilon_{mel}$ ) and the dominant eumelanin was used. For some of the volunteers, specifically those from southern Asian descent, significant poorer fit results were obtained for the measured  $R_p$  data. Further investigations led to the postulation that the melanin parameter in Eq. 4.4 should account for both the eumelanin and pheomelanin contributions. Eq. 4.4 was then rewritten to explicitly be dependent on both types of melanin:

$$\mu_a(\lambda) = c_{HbO_2}[\alpha\varepsilon_{HbO_2}(\lambda) + (1 - \alpha)\varepsilon_{Hb}(\lambda)] + c_{Eu}\varepsilon_{Eu}(\lambda) + c_{Pheo}\varepsilon_{Pheo}(\lambda) \quad (4.7)$$

with:

$c_{Eu}$  = eumelanin concentration

$c_{Pheo}$  = pheomelanin concentration

$\varepsilon_{Pheo}(\lambda)$  = extinction coefficient for pheomelanin (Jacques SL, 1998(a))

$\varepsilon_{Eu}(\lambda)$  = extinction coefficient for eumelanin (Jacques SL, 1998(a))

and others as used in Eq. 4.4

The measured probe reflectance can now be described mathematically in terms of six coefficients ( $c_{HbO_2}$ ,  $\alpha$ ,  $c_{Eu}$ ,  $c_{Pheo}$ ,  $c_d$ ,  $\mu'_s(\lambda_{min})$ ) that are adjusted to best match the equation to the experimental data. The data and fit results of three different volunteers are shown in Figure 4.2 for the two models. Model A2 (Eq 4.4 for  $\mu_a$ ) only uses a single melanin parameter and model D2 (Eq. 4.7 for  $\mu_a$ ) uses both the eumelanin and pheomelanin parameters. There is a definite improvement when model D2 is used on the medium skin phototype (Asian descent) without negative impact on the other skin phototypes.

The ability of the algorithm to separate the coefficients was tested by generating a curve with 6 coefficients with some random noise, representative of typical measured  $R_p$  values. The algorithm was then applied to the curve in the same manner that it was used on the measured data. In Table 4.1 the fitted parameters are compared with the input data to the curve and the typical fitted curves are shown in Figure 4.3.

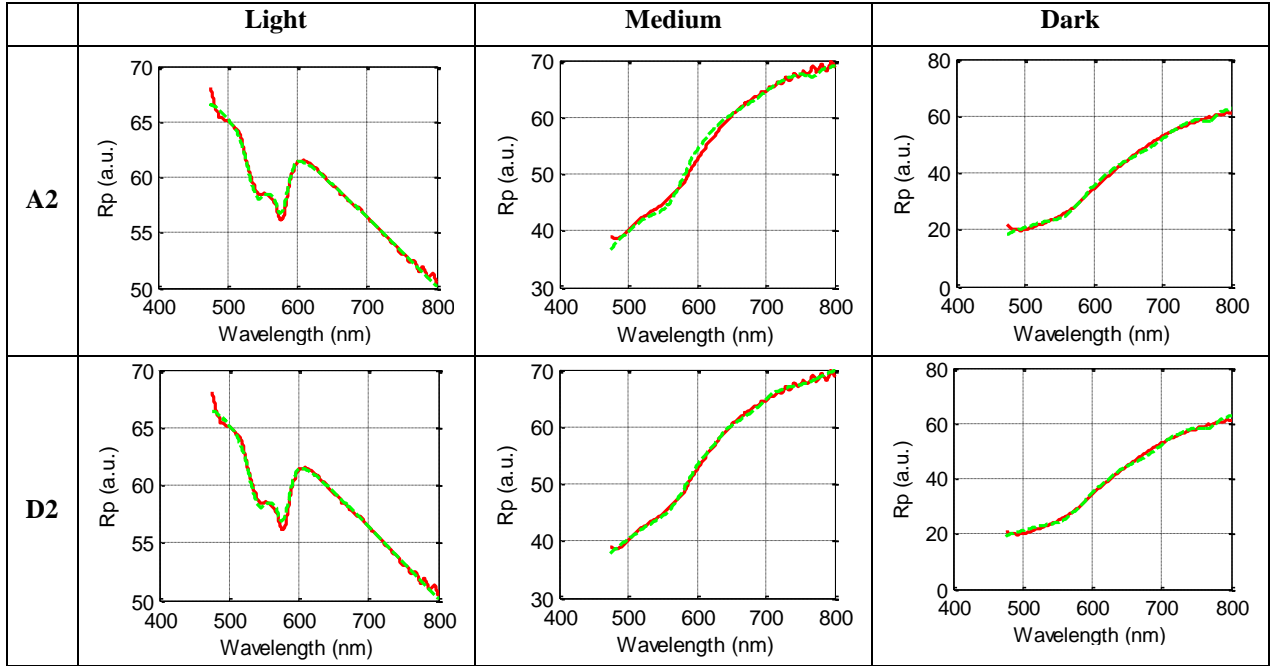


Figure 4.2: Comparing the two different melanin models for three volunteers each representing a different skin phototype. Model A2 only uses a single melanin parameter and model D2 uses both eumelanin and pheomelanin. Solid lines (—) represent the experimental data and the dashed lines (---) the fitted curve.

Table 4.1: Fitted parameters as compared to the input parameters into the algorithm.

Parameter	Set 1		Set 2	
	Input	Fitted	Input	Fitted
1	$3.20000 \times 10^{-5}$	$3.19565 \times 10^{-5}$	$8.00000 \times 10^{-5}$	$7.87171 \times 10^{-5}$
2	$1.00000 \times 10^{-2}$	$1.66647 \times 10^{-2}$	$7.00000 \times 10^{-1}$	$7.18282 \times 10^{-1}$
3	$7.75600 \times 10^{-3}$	$7.55275 \times 10^{-3}$	$8.00000 \times 10^{-3}$	$7.80733 \times 10^{-3}$
4	$2.60000 \times 10^{-4}$	$2.79790 \times 10^{-4}$	$2.00000 \times 10^{-3}$	$2.04942 \times 10^{-3}$
5	$1.00000 \times 10^0$	$9.99749 \times 10^{-1}$	$4.00000 \times 10^{-1}$	$3.96303 \times 10^{-1}$
6	$1.58000 \times 10^0$	$1.57090 \times 10^0$	$2.00000 \times 10^0$	$1.97998 \times 10^0$

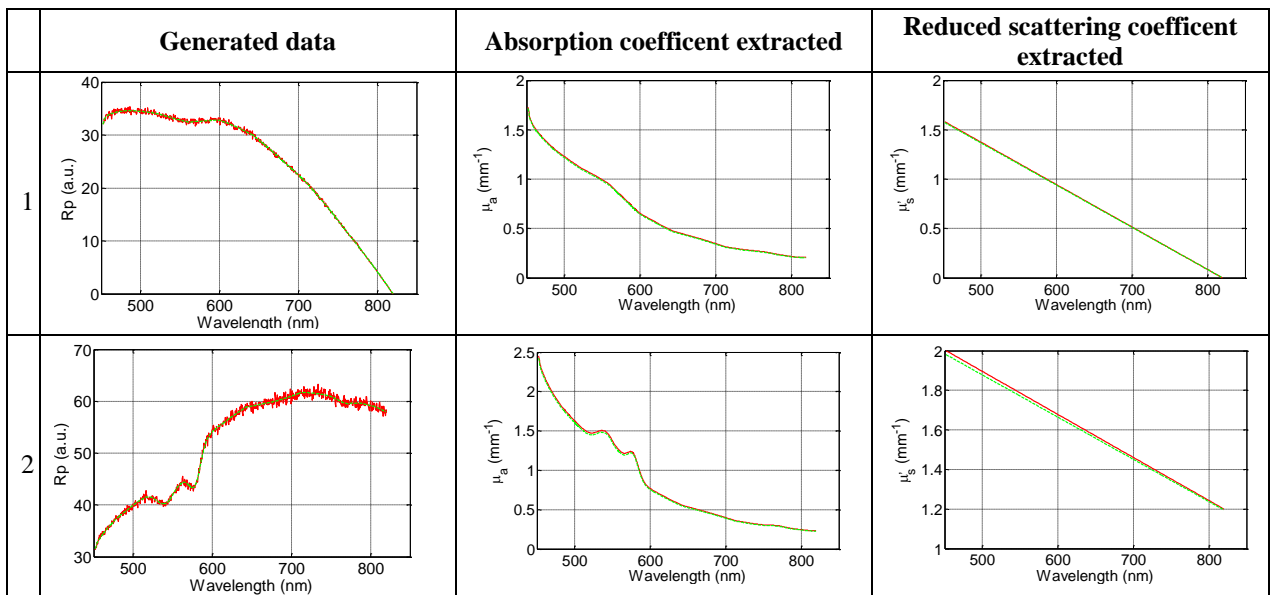


Figure 4.3: Comparison of input values to the fitted values for two different test cases. Solid lines (—) represent the input data and the dashed lines (---) the fitted curve.

## 4.2 PROBE CALIBRATION

An integrated diffuse reflectance probe (DRP) (R200-7-UV-VIS from Ocean Optics Inc. Florida, USA) was used in the experiments. The optimal transmission of the probe is between 250 and 800 nm. The probe contains seven fibres each with a diameter of 200  $\mu\text{m}$ . Six fibres arranged in a ring are used for light delivery and the 7<sup>th</sup> fibre in the centre of the probe is used to collect the diffuse reflected light (Figure 2.13 in section 2.4.2). A halogen white light source (HL-2000, Ocean Optics Inc. Florida, USA) emitting between 450 and 900 nm was used as illumination source. The reflected light is collected in the central fibre and used as input to an USB-4000 spectrometer (also from Ocean Optics). A reflectance standard, WS-1 Spectralon (Ocean Optics Inc. Florida, USA), was used to calibrate the reflectance probe for each set of experiments.

A set of 60 liquid calibration phantoms, consisting of IL and black ink, were prepared. This is different to the calibration phantoms used by other DRP users, but is a well-recognised procedure for preparing skin simulating phantoms (Star WM, 1988), (van Staveren HJ, 1991), (Farrel TJ, 1992), (Flock S, 1992), (Michielsen K, 1998). In the original paper (Zonios G, 2006) the calibration tissue phantoms were prepared by using 1.0  $\mu\text{m}$  diameter polystyrene beads (suspended in deionised water) and haemoglobin from bovine blood prepared in distilled water. For the calibration of the DRP in this work the IL+ink phantom solutions were poured into transparent 6-well cell culture plates (Lasec SA) with a diameter of  $\sim 35$  mm. The same phantom preparation procedures were followed here as for the liquid phantoms used in the computer model calibration as discussed in section 3.5 which contains the paper on the experimental verification of the computer model.

The thickness of the phantoms in the culture plates was about 10 mm. The culture plates were placed on a black paper during the experiments to ensure that no light is reflected from the table surface. Visual inspection in a dark room also indicated that no light was leaving the phantoms through the sides. Calibrations were performed in a laboratory where the temperature was kept between 22 and 23  $^{\circ}\text{C}$ . The experimental setup as used for both the calibration and the volunteers are shown in Figure 4.4.

A Z-translation stage was used to hold the probe in a vertical position, facing downwards. The probe was lowered until it just entered into the liquid phantom.

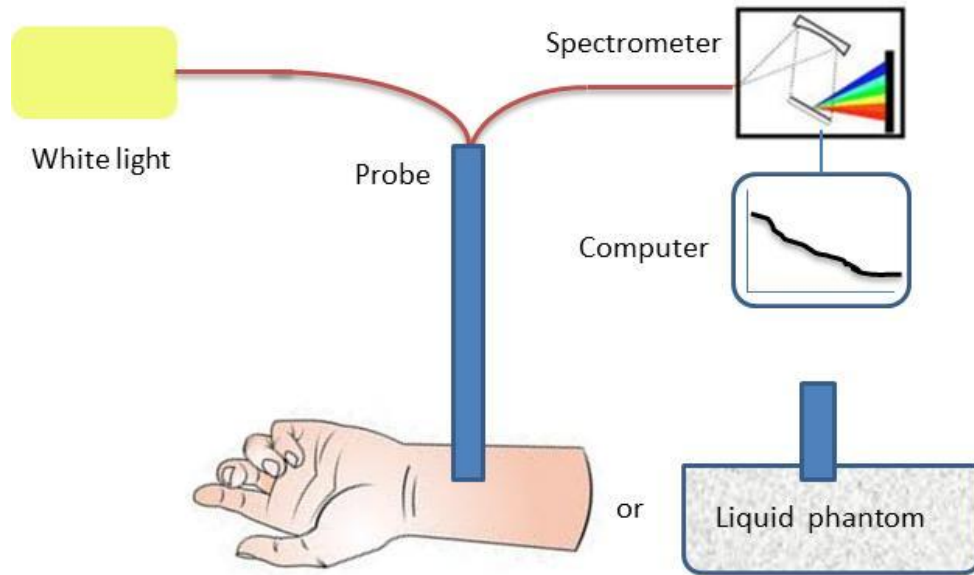


Figure 4.4: Experimental setup for calibration and *in vivo* tests.

All the evaluations were done at two wavelengths, 633 and 676 nm. These wavelengths were chosen for the applicability to PDT (676 nm) and the data available in literature for HeNe lasers ( $\lambda=632.8$  nm). For the phantoms the values of  $\mu_a$  were limited to between 0.068 and  $2.479 \text{ mm}^{-1}$  due to practical considerations in transmission through the phantoms. For high  $\mu_a$  the transmitted power became too low for accurate measurements. The optical path length for the cuvette used in the absorption measurements was 1.22 mm. In the calibration work  $\mu'_s$  was restricted between 0.539 and  $3.558 \text{ mm}^{-1}$ .

Before each set of experiments, the system was calibrated with the WS-1 reflectance standard. The standard was placed 5 mm from the end of the probe tip. This method was described by Zonios (Zonios G, 2008(a)). The DRP could not be placed in contact with the standard as this resulted in saturation of the detector during the reflectance standard measurements. Great care was taken during the experiments to ensure that the standard was always placed the same distance from the probe's end, by using the Z-translation stage to position the probe vertically.

The basic calibration procedure as described by Zonios (Zonios G, 2006) was followed to extract the probe's geometrical calibration constants  $k_1$  and  $k_2$ . The calibration constants were then used in the optimising algorithm to extract the  $\mu_a$  and  $\mu'_s$  values from measured data on the 30 volunteers.

The calibration process and control experiments are further described in the paper in section 4.2.1. In the calibration work two laser wavelengths (633 and 676 nm) were used in all the comparisons.

#### **4.2.1 Paper on Reflectance probe calibration**

The paper on the calibration of the reflectance probe was published online on 13 March 2012 in Lasers in Medical Science:

[<http://www.springerlink.com/content/e037471262313654/fulltext.html>].

As discussed in section 3.5, minor formatting changes have been made to the paper to follow the style of the thesis.

## Diffuse reflectance spectroscopy as a tool to measure the absorption coefficient in skin: system calibration

A E Karsten<sup>1,2</sup>, A Singh<sup>1</sup>, P A Karsten<sup>3</sup>, M W H Braun<sup>2</sup>

<sup>1</sup> Biophotonics Group, National Laser Centre, CSIR, P. O. Box 395, Pretoria, 0001, South Africa

<sup>2</sup> Department of Physics, University of Pretoria, Pretoria, 0002, South Africa

<sup>3</sup> Ballistics Research Group, Denel Land Systems, P O Box 7710, Pretoria, 0001, South Africa

### ABSTRACT

An individualised laser skin treatment may enhance the treatment and reduces risks and side-effects. The optical properties (absorption and scattering coefficients) are important parameters in the propagation of laser light in skin tissue. The differences in the melanin content of different skin phototypes influence the absorption of the light. The absorption coefficient at the treatment wavelength for an individual can be determined by diffuse reflectance spectroscopy, using a probe containing 7 fibres. Six of the fibres deliver the light to the measurement site and the central fibre collects the diffused reflected light. This is an *in vivo* technique, offering benefits for near real time results. Such a probe, with an effective wavelength band from 450 nm-800 nm, was used to calibrate skin-simulating phantoms consisting of intralipid and ink. The calibration constants were used to calculate the absorption coefficients from the diffuse reflectance measurements of three volunteers (skin phototypes, II, IV and V) for sun exposed and non exposed areas on the arm.

**Keywords:** diffuse reflectance, absorption coefficient, skin-simulating phantom

### INTRODUCTION

Lasers and other light sources offer non-invasive benefits both in terms of diagnostic and treatment modalities. For most non-invasive laser procedures, light must penetrate through some skin layers before reaching the diagnostic or treatment site. The absorption and scattering of laser light are the two major interactions that reduce the laser light intensity as it passes through human skin. The major contributors to the absorption of light in human skin are haemoglobin (both oxyhaemoglobin and deoxyhaemoglobin) and melanin, present in the epidermal layer. Scattering is mainly the result of the sub-cellular structures. The three most important properties for describing the propagation of light through tissue are the absorption ( $\mu_a$ ) and scattering ( $\mu_s$ ) coefficients as well as the anisotropy ( $g$ ). In order to reduce the complexity, the last two parameters are usually combined as the reduced scattering coefficient ( $\mu'_s = (1 - g)\mu_s$ ) (Pfefer TJ, 2003), (Martelli F, 2010).

In individualising laser treatment, the absorption and scattering properties at the treatment locale of the patient must be known. Due to the variance in the available data and the limited data available in open literature, it became important to measure the absorbance of different skin phototypes in the research laboratory. One of the non-invasive methods that can be used to determine  $\mu_a$  and  $\mu'_s$  is diffuse reflectance spectroscopy, a method that detects light that has been scattered multiple times within the sample (skin) under investigation. (Johns M, 2005), (Zonios G, 2006), (González FJ, 2010). The method was successful in identifying the change in a melanin index for specific skin conditions.

Epidermal melanin is responsible for skin phototype or skin tone (Costin GE, 2007). Melanin in the skin is located in the melanosomes and consists of solid absorbing particles with a diameter between 20-40 nm. It is an optically dense material which absorbs radiation in the visible wavelength range. Melanin is not a single pigment, but is composed of a number of different chromophores with varying optical and physical properties (Alaluf S, 2001). Melanin can broadly be divided into two families according to chemical structure and colour (Agache P, 2004). Eumelanins are black-brown in colour and are sulphur poor, while pheomelanins are yellow-reddish in colour and sulphur rich (Agache P, 2004), (Costin GE, 2007).

The composition of melanin in an individual depends on both genetic and environmental factors. Eumelanin provides better photo protection than pheomelanin. In healthy, photo-exposed skin, the distribution of melanin is different depending on whether it was exposed to UVA, UVB or PUVA (Psoralen + UVA, a treatment for psoriasis, eczema and vitiligo). Exposure to UVB radiation increases the production of melanin and the transfer into keratinocytes. This leads to an increase in the concentration of melanin in the epidermis. After UVA exposure, a large amount of melanin is found in melanocytes and keratinocytes of the basal layer, but the melanin concentration in the rest of the epidermis remains unchanged (Agache P, 2004).

This paper describes the calibration process for a diffuse reflectance probe system on a set of liquid calibration phantoms prepared from intralipid (IL) and black ink. The calibrated system is then used to deduce the absorption coefficient from measurements on three individuals with different skin phototypes (skin phototypes II, IV and V on the Fitzpatrick scale (Fitzpatrick TB, 1988)). Ethics approvals for these measurements were obtained from both the University of Pretoria (EC110830-060) and the CSIR (Ref 17/2011).

## MATERIALS AND METHODS

### Diffuse reflectance measurements

Light that enters the skin is scattered due to various processes. The most important processes are the changes in optical density between different layers (refractive index changes), Mie scattering (scattering where the scattering particles are of the order of the photon wavelength) and Rayleigh scattering (scattering of light by structures much smaller than the photon wavelength). Some of the light is scattered back in the direction from where it entered and leaves the skin (see Figure 4.5). This diffusely reflected light can be collected and measured with a fibre optic based diffuse reflectance probe (see Figure 4.6).

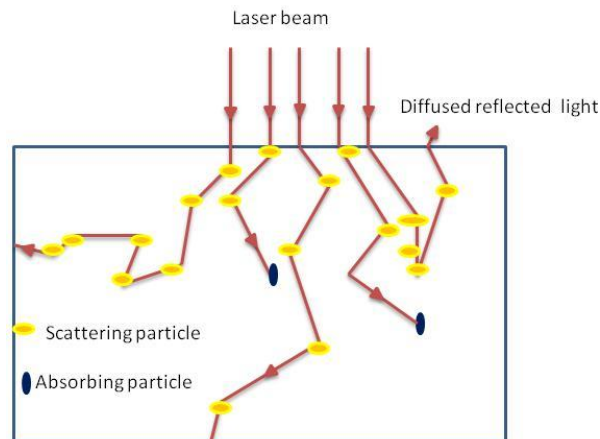


Figure 4.5: Absorption and scattering in skin.

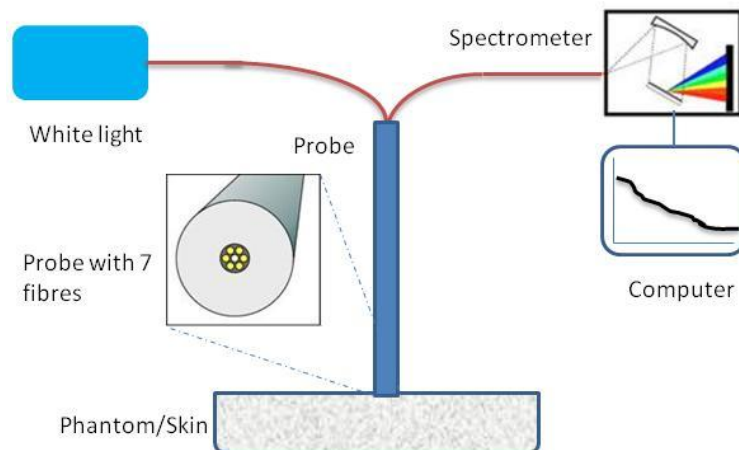


Figure 4.6: Experimental setup.

A diffuse reflectance probe usually consists of a few optical fibres grouped together. A typical configuration consists of 7 optical fibres, with 6 light transmitting fibres arranged around the central collecting fibre. The signal collected by the central fibre is used as the input to a spectrometer. The diffused back reflected signal as a function of wavelength is recorded on a computer.

The diffuse reflectance spectra measured with the optical probe contain entangled information regarding the scattering and absorption of light in tissue (Zonios G, 2006). A spectral analysis model describing the diffuse reflectance in terms of these optical properties was proposed by Zonios (Zonios G, 2006). This is an inverse model, starting with the measured diffuse reflectance spectrum to calculate the reduced scattering coefficient ( $\mu'_s$ ) and the absorption coefficient ( $\mu_a$ ) of the skin sample measured. To minimize mathematical complexity, the skin is modelled as a semi-infinite turbid medium. Zonios tested the validity of the model on tissue-simulating phantoms and with the analysis of diffuse reflectance spectra from human skin *in vivo* (Zonios G, 2006).

Due to the limitation imposed by measurements with a diffuse reflectance probe, the diffuse reflectance can be expressed by an explicit dependence on  $\mu'_s$  (Zonios G, 2006). The reflectance probe backscattered signal ( $R_p$ ) can be described by (Zonios G, 2006):

$$R_p(\lambda) = \frac{\mu'_s(\lambda)}{k_1 + k_2\mu_a(\lambda)} \quad (4.8)$$

where  $k_1$  and  $k_2$  are parameters that depend on the probe geometry and need to be calculated from the probe calibration data.

The absorption coefficient ( $\mu_a$ ) as a function of wavelength is given by:

$$\mu_a(\lambda) = c_{HbO_2}[\alpha\varepsilon_{HbO_2}(\lambda) + (1 - \alpha)\varepsilon_{Hb}(\lambda)] + c_{Eu}\varepsilon_{Eu}(\lambda) + c_{Pheo}\varepsilon_{Pheo}(\lambda) \quad (4.9)$$

and the reduced scattering coefficient ( $\mu'_s$ ) by:

$$\mu'_s(\lambda) = \left[1 - c_d \left(\frac{\lambda - \lambda_1}{\lambda_2 - \lambda_1}\right)\right] \mu'_s(\lambda_{min}) \quad (4.10)$$

with:

$\varepsilon_{HbO_2}(\lambda)$  = extinction coefficient for oxyhaemoglobin (Prahl S, 1999)

$\varepsilon_{Hb}(\lambda)$  = extinction coefficient for deoxyhaemoglobin (Prahl S, 1999)

$\varepsilon_{Eu}(\lambda)$  = extinction coefficient for eumelanin (Jacques S, 2001)

$\varepsilon_{Pheo}(\lambda)$  = extinction coefficient for pheomelanin (Prahl S, 1999)

$c_d$  = parameter related to melanin particle size

$c_{HbO_2}$  = oxyhaemoglobin concentration

$c_{Hb}$  = deoxyhaemoglobin concentration

$\alpha$  = oxygen saturation level of blood, defined as the percentage of the oxygenated blood of the total blood concentration  $\alpha = \frac{c_{HbO_2}}{c_{HbO_2} + c_{Hb}}$

$\lambda_1$  = min ( $\lambda$ )

$\lambda_2$  = max ( $\lambda$ )

Eq. 4.10 describes a linear dependence of the reduced scattering coefficient on the wavelength. This is a reasonable approximation which is supported by Mie theory calculations for spherical scatterers with a Gaussian distribution in size (Zonios G, 2001).

### Experimental methods

The liquid phantoms were prepared from a mixture of 20% Intralipid (IL) (Sigma Aldrich, lot # 028K0740) and black ink (Trodar colour 7011). IL and ink are often used as optical simulants for human skin (van Staveren HJ, 1991), (Flock S, 1992). More detail on the phantom preparations can be found in (Karsten AE, 2012(a)).

A diffuse reflectance probe from Ocean Optics is used in the experiments. The illumination is done with a white-light source through the outer fibre ring and the diffused reflected data is collected through the centre fibre as illustrated in Figure 4.6. The diffuse reflectance probe system consists of the following components (see Figure 4.6):

- Diffuse reflectance probe, 5 mm outer diameter, (R200-7-UV-VIS, optimal transmission between 250-800 nm) with fibre diameter 200  $\mu\text{m}$  (Ocean Optics). The probe contains 7 fibres, 6 fibres in a ring for light delivery and the 7th fibre in the centre of the probe to collect the diffuse reflectance spectrum.
- Halogen white light source (HL-2000) emitting between 450 and 900 nm (Ocean Optics).
- USB-4000 spectrometer (Ocean Optics) sensitive between 350 nm and 1000 nm.
- Computer.
- WS-1 Spectralon reflectance standard (Ocean Optics), used to calibrate the reflectance data for each set of experiments.

Matching the wavelength transmission through the different components of the system results in an effective wavelength band from 450 nm-800 nm.

Before each set of experiments, the system was calibrated with the WS-1 reflectance standard and a calibrated solid phantom (reference phantom with known optical properties) to ensure proper operation of all the components of the system.

During phantom experiments, the probe was inserted, from the top, into the solution eliminating intralipid-air interfaces for the probe. The probe tip was facing vertically down towards the bottom of the container just touching the liquid.

Raw data collected by the probe was corrected for the detector dark current and normalised with respect to the white reflecting standard (WS-1) according to eq. 4.11. The Reflectance wizard in the Spectra Suite software from Ocean Optics was used to measure the back reflected light.

$$R_p(\lambda) = -\log_{10} \left[ \frac{I_{meas}(\lambda) - I_D(\lambda)}{I_{ref}(\lambda) - I_D(\lambda)} \right] \quad (4.11)$$

where:

- $I_{meas}(\lambda)$  = raw reflection data
- $I_D(\lambda)$  = detector dark current
- $I_{ref}(\lambda)$  = spectrum obtained from WS-1

All the measurements were done with the main lights in the laboratory switched off and only a reading lamp for lighting. During the experiments the light was turned away, to ensure that there is no interference from the light. This was tested by comparing spectra with the reading light turned away and spectra with the reading light switched off. The spectra were identical. The temperature in the laboratory was maintained between 22 and 23 °C.

### Calibration phantoms

Skin-simulating liquid phantoms consist of a mixture of IL and ink. The assumption is made that the IL does not absorb light and that the ink does not scatter light in the wavelength range used in this study. The IL and ink samples were prepared separately and characterised before mixing the IL and ink to form the skin-simulating phantoms used for calibration of the system. Each phantom consisted of 5 ml IL solution and 5 ml ink solution mixed together to form a 10 ml phantom. Eleven IL solutions and twenty ink solutions were prepared. Three of the IL solutions were mixed with the twenty ink solutions to form a 3x20 calibration matrix. The solutions were poured into transparent 6-well cell culture plates (Lasec SA) with a diameter of ~35 mm. The depth of the solution was ~10 mm. The 6 well plates were used to ensure that there are no interference from light reflected from the sides and bottom of the plate (semi infinite layer assumption). The plates were placed on a black absorbing surface and the probe was lowered with a translation stage to just touch the surface of the liquid phantom. An 8 mW HeNe laser ( $\lambda=632.8$  nm from Spectraphysics) and a locally constructed diode laser ( $\lambda=676$  nm) with output power 25 mW were used in the absorption measurement of the ink solutions.

The different IL concentrations used for the phantoms and the corresponding  $\mu'_s$  values (calculated from (Michielsen K, 1998)) are listed in Table 4.2. Absorption through the ink samples were measured with both lasers on three separate days. The Beer-Lambert law was used to calculate the  $\mu_a$  values for the different ink solutions listed in Table 4.3. The ink absorption values were averaged for the three measurements and the standard deviations calculated (Microsoft Excel 2007 calculations), are reported in Table 4.3. The range of  $\mu_a$  and  $\mu'_s$  values used were selected to cover the typical published  $\mu_a$  and  $\mu'_s$  values for skin (Tuchin V, 2007).

Table 4.2: IL concentrations and corresponding  $\mu'_s$  values at  $\lambda = 632$  and  $676$  nm.

IL sample	IL concentration (%/vol)	$\mu'_s$ at $\lambda = 632$ nm ( $\text{mm}^{-1}$ )	$\mu'_s$ at $\lambda = 676$ nm ( $\text{mm}^{-1}$ )
1	0.500	0.624	0.593
2	0.750	0.936	0.890
3	1.000	1.248	1.186
4	1.250	1.560	1.483
5	1.500	1.872	1.779
6	1.750	2.184	2.076
7	2.000	2.496	2.372
8	2.250	2.808	2.669
9	2.500	3.120	2.965
10	2.750	3.432	3.262
11	3.000	3.744	3.558

Table 4.3: Ink sample and the  $\mu_a$  values calculated with the Beer-Lambert law using the transmission measurements.

Ink sample	$\lambda = 632$ nm		$\lambda = 676$ nm	
	Average $\mu_a$ ( $\text{mm}^{-1}$ )	Standard deviation	Average $\mu_a$ ( $\text{mm}^{-1}$ )	Standard deviation
1	0.126	0.011	0.068	0.001
2	0.199	0.010	0.099	0.028
3	0.289	0.014	0.153	0.066
4	0.359	0.019	0.196	0.120
5	0.496	0.010	0.277	0.060
6	0.613	0.009	0.326	0.057
7	0.620	0.015	0.341	0.068
8	0.753	0.020	0.412	0.238
9	0.849	0.022	0.465	0.078
10	0.968	0.017	0.533	0.062
11	1.305	0.018	0.758	0.094
12	1.576	0.015	0.844	0.062
13	1.695	0.016	0.805	0.026
14	2.372	0.261	1.635	0.003
15	2.114	0.015	1.224	0.071
16	2.372	0.017	1.219	0.062
17	2.524	0.027	1.405	0.117
18	2.842	0.046	1.688	0.100
19	3.222	0.022	1.928	0.533
20	3.737	0.024	2.479	0.325

To evaluate the dependence of the diffuse reflectance ( $R_p$ ) as a function of  $\mu'_s$ , the eleven IL concentrations listed in Table 4.2 were used. Three IL samples (2, 6 and 11) were used in combination with the 20 ink samples to prepare 60 phantoms.

In order to extract the  $\mu_a$  values from the liquid phantoms, the extinction coefficient of the ink must be known. This can be derived via absorbance measurements. In order to verify the experimental procedure to extract the extinction coefficient, neutral density absorbing filters (OD = 0.2, 0.4 and 0.6) from Thor Labs were

used as ‘absorbers’. The neutral density filters do not have scattering materials and only act as absorbers. The filters were placed in-between the 676 nm laser and an Ophir power meter. The absorption coefficient was calculated by using the Beer-Lambert law.

$$I_a = I_0 e^{-\mu_a d} \quad (4.12)$$

with:

$I_a$  = light intensity after the ink/filter

$I_0$  = intensity from light/laser source

$d$  = optical path length (mm)

The absorbance was also measured with the Absorbance wizard in the SpectraSuite software from Ocean Optics. The extinction coefficient for each filter was then calculated from the absorbance data and used to calculate  $\mu_a$  by rewriting eq. 4.9 as

$$\mu_a(\lambda) = c_{filter} \varepsilon_{filter}(\lambda) \quad (4.13)$$

reflecting the absence of haemoglobin and the filter absorbance as substitute for melanin. The absorbance ( $A(\lambda)$ ), as measured by the Absorbance wizard is given by:

$$A(\lambda) = -\log_{10} \left( \frac{I_a(\lambda) - I_D(\lambda)}{I_0(\lambda) - I_D(\lambda)} \right) = OD \quad (4.14)$$

with:

$I_a(\lambda)$  = signal with the ink/filter

$I_0(\lambda)$  = signal from light source without ink/filter

$I_D(\lambda)$  = detector dark current as a function of wavelength

$OD$  = optical density

The absorption coefficient from the Absorbance wizard can then be calculated by:

$$\mu_a(\lambda) = -\left(\frac{1}{d}\right) \ln(10^{-A(\lambda)}) \quad (4.15)$$

Good agreement was found between the  $\mu_a$  values calculated using the Beer-Lambert law and the Absorbance wizard measurements. The results are listed in Table 4.4.

Table 4.4: Comparison between the different methods to calculate  $\mu_a$  for the neutral density absorbing filters at a wavelength of 676 nm.

Optical Density (from supplier @ 633 nm)	0.2	0.4	0.6
Optical Density (calculated @ 633 nm)	0.1859	0.3967	0.6019
Filter thickness (mm)	1.35	0.74	1.30
$I_0$ (mW)	25.6	25.8	26.4
$I_a$ (mW) after filter	16.5	10.6	7.0
$\mu_a$ (mm <sup>-1</sup> ) (Beer-Lambert)	0.3254	1.2021	1.0211
$\mu_a$ (mm <sup>-1</sup> ) (Absorbance wizard)	0.3035	1.1307	0.9799

The absorbance measured for the different filters as a function of wavelength is shown in Figure 4.7(a). The optical density (OD) for each filter is given in the graph and compares well with the suppliers specified OD at a wavelength of 633 nm. It shows very good correlation with the OD calculated from the Absorbance wizard measurements.

The same procedure was repeated to calculate the extinction coefficient of the ink. This derived ink extinction coefficient was then used to calculate  $\mu_a$  from the reflectance probe data in the phantoms (IL+ink). The result of the data points that adhere to the condition ( $\mu_a < \mu'_s$ ) are plotted in Figure 4.7(b) where the  $\mu_a$  values calculated from the reflectance probe measurements are compared to the true  $\mu_a$  values as per Table 4.3.

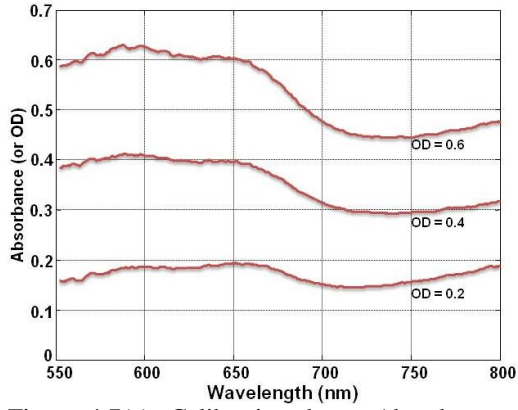


Figure 4.7(a): Calibration data - Absorbance as function of the wavelength for the different OD filters.

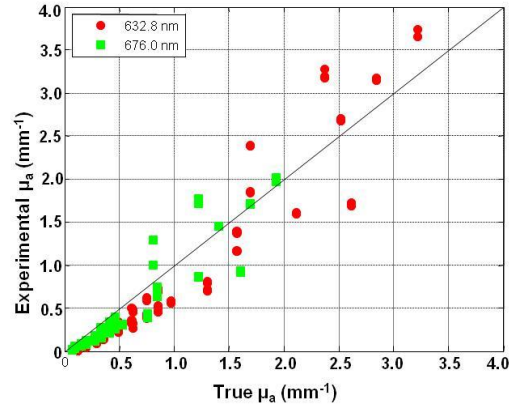


Figure 4.7(b): Calibration data -  $\mu_a$  values extracted from the DRP measurements compared to the true  $\mu_a$  values (measured using the beer Lambert law) of the ink phantoms.

### Diffuse Reflectance probe measurements on skin

Reflectance measurements were done on three South African volunteers with skin phototypes II, IV and V. The probe was placed on the measurement site, just touching the skin. Two different skin sites were measured on each volunteer:

- Inside upper arm (no/little sun exposure)
- Outside lower arm (sun exposed)

At each position three measurements were taken within a two minute period. All measurements were done on the same day. For both the skin data and the calibration data, the integration time for the probe measurements were 20 ms and the signal was averaged 4 times.

### Data analysis

The MATLAB function LSQCURVEFIT was used to solve eq. 4.8 in a least-squares sense using nonlinear curve-fitting. The measured probe reflectance is described mathematically in terms of 6 coefficients ( $c_{HbO_2}$ ,  $\alpha$ ,  $c_{Eu}$ ,  $c_{Pheo}$ ,  $c_d$ ,  $\mu'_s(\lambda_{min})$ ) that are adjusted to best match the equation to the experimental data. The function requires an initial estimate of the parameters to be optimized and has the option to include bound constraints. According to the MATLAB documentation the algorithm is a subspace trust-region method and is based on the interior-reflective Newton method described in (Coleman T, 1994), (Coleman T, 1996), where each iteration involves the approximate solution of a large linear system using the method of preconditioned conjugate gradients (PCG).

## RESULTS AND DISCUSSIONS

The skin-simulating liquid phantoms were used to determine the probe geometry calibrations constants  $k_1$  and  $k_2$  in eq. 4.8. Figure 4.8(a) shows the linear dependence of the reflectance probe values  $R_p$  on  $\mu'_s$ . This is consistent with data published by other authors using fibre optic probes to measure the diffused back reflectance (Amelink A, 2004), (Johns M, 2005), (Zonios G, 2006). The results are also consistent with previous findings that the linear dependence of  $R_p$  on  $\mu'_s$  is only valid for  $\mu'_s$  up to  $3.2 \text{ mm}^{-1}$  (Zonios G, 2008(a)).

The dependence of  $R_p$  on  $\mu_a$  exhibits the expected monotonic behaviour (Figure 4.8(b)). Diffused reflectance measurements for three different  $\mu'_s$  values, namely  $0.89$ ,  $2.076$  and  $3.558 \text{ mm}^{-1}$ , were fitted to eq. 4.8. Table 4.5 shows the fit results.

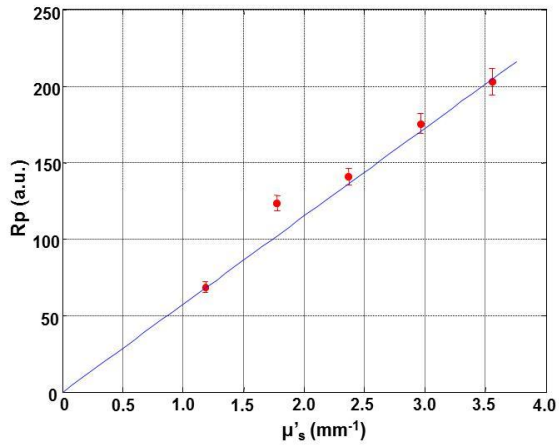


Figure 4.8(a): Reflectance probe measurement as a function of  $\mu'_s$  at  $\lambda=676$  nm when only IL was used ( $\mu_a = 0$ ).

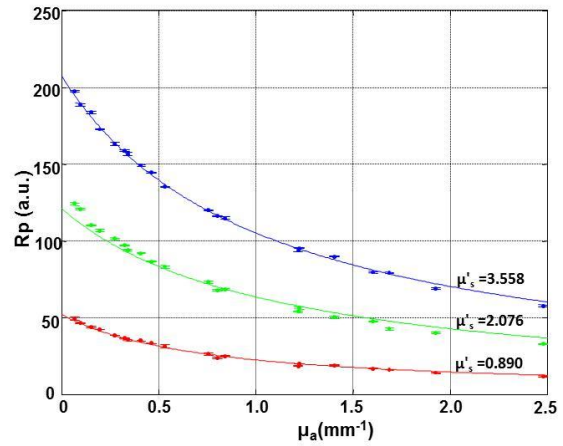


Figure 4.8(b): Reflectance probe measurement as a function of  $\mu_a$  at a  $\lambda=676$  nm for three different  $\mu'_s$  solutions.

Table 4.5: Geometrical parameters ( $k_1$  and  $k_2$ ), calculated from the reflectance measurements of the IL+ ink phantoms in Figures 4.8(a) and 4.8(b).

	$k_1$	$k_2$
Min	0.015247	0.015407
Max	0.017333	0.025437
Mean	0.016312	0.019144

### Skin measurements

Diffused reflectance as a function of wavelength is shown in Figure 4.9(a) for all three individuals. In some cases the three separate measurement lines are distinguishable (e.g. Type II Not exposed), but in other cases not (e.g. Type II sun exposed). The three measurements for each individual were averaged for the data analysis. Using eq. 5.8, the  $\mu_a$  values at wavelengths 633 nm and 676 nm were extracted and are shown in Figure 4.9(b). The data was analysed for the minimum, maximum and mean  $k_1$  and  $k_2$  values. The average values were plotted in Figure 4.9(b) and the error bars indicate the standard deviation of the data. For clarity, the values are also listed in Table 4.6.

Table 4.6: Absorption coefficients calculated using the mean  $k_1$  and  $k_2$  values for the different skin types at wavelengths of 633 nm and 676 nm.

Skin phototype	$\mu_a$ (mm <sup>-1</sup> ) Sun exposed		$\mu_a$ (mm <sup>-1</sup> ) Non exposed	
	633 nm	676 nm	633 nm	676 nm
II	0.0157	0.0112	0.0041	0.0021
IV	0.509	0.400	0.205	0.161
V	1.39	1.04	0.896	0.703

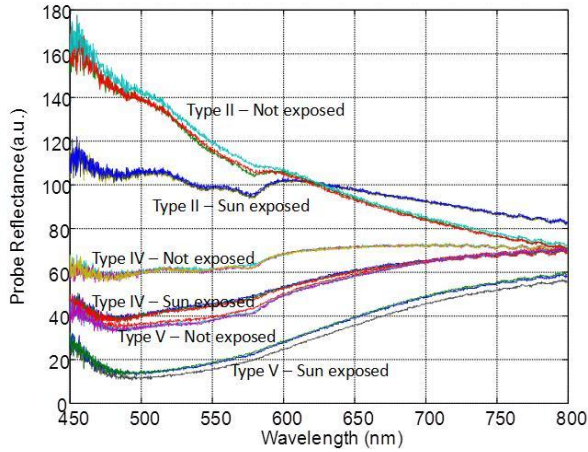


Figure 4.9(a): Reflectance probe measurements on three individuals with skin phototype II, IV and V. Three measurements were taken on both the lower outer arm (sun exposed) and the inner upper arm (not sun exposed).

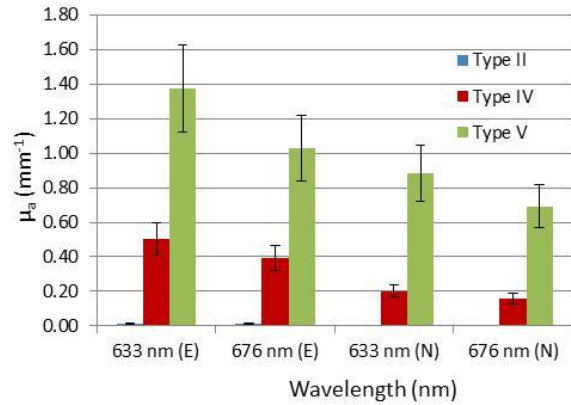


Figure 4.9(b): Absorption coefficient values calculated from the reflection probe measurements for three different skin phototypes at wavelengths 633 nm and 676 nm on sun exposed (E) and non-exposed (N) parts of the arm.

## CONCLUSIONS

Most papers reporting on the diffuse reflectance probe technique do not provide values for the absorption coefficient. Great care was taken in ensuring that the calibration models were set up correctly due to the influence of the calibration constants ( $k_1$  and  $k_2$ ) on the results. Originally all 60 IL+ink phantoms were used to compare the calculated absorption coefficient obtained using the reflectance probe to the absorption coefficient of the ink calculated using the Beer-Lambert law. The deviations were greatly reduced when only data points compliant with the diffusion condition  $\mu_a < \mu'_s$ , were used (Star WM, 1997), (Zonios G, 2001). The variance in the data was larger than anticipated, but when compared to other publications, the error bars are comparable (Tseng S, 2009).

*In vivo* skin measurements remain a challenge. The detection fibre in the reflectance probe has a diameter of only 200  $\mu\text{m}$ . During the skin measurements the probe was held in position on the same spot, but due to blood flow, breathing, unsteadiness of the volunteers, it is not easy to ensure that all three measurements were done under exactly the same conditions. Despite the limitations, relatively good agreement was found with Simpson (Simpson R, 1998(a)) where *ex vivo* skin samples were measured on an Integrating Sphere. Simpson used sample from areas of the skin that are not normally exposed to the sun. They measured  $\mu_a$  values, at a wavelength of 633 nm, of around 0.035  $\text{mm}^{-1}$  for ‘caucasian’ skin and 0.25  $\text{mm}^{-1}$  for ‘negroid’ skin. Tseng (Tseng S, 2009) measured  $\mu_a$  values of 0.060  $\text{mm}^{-1}$  (for skin type I-II), 0.062  $\text{mm}^{-1}$  (for skin type III-IV) and 0.071  $\text{mm}^{-1}$  (for skin type V-VI) for the upper inner arm (not sun exposed) and 0.063  $\text{mm}^{-1}$  (for skin type I-II), 0.065  $\text{mm}^{-1}$  (for skin type III-IV) and 0.074  $\text{mm}^{-1}$  (for skin type V-VI) for the dorsal arm (sun exposed).

In order to quantify the absorption coefficient for the range of the South African skin types a clinical test with more volunteers needs to be conducted. The results of such a study will enable laser users in the medical profession to individualise laser skin treatments.

## Acknowledgements

The authors would like to acknowledge Mr Bafana Moya for the work in the laboratories.

## References

- Agache P, Humbert P. *Measuring the skin*. ISBN 3-540-01771-2. Springer-Verlag, 2004.
- Alaluf S, Heath A, Carter N, Atkins D, Mahalingam H, Barrett K, Kolb R, Smit N. "Variation in Melanin Content and Composition in Type V and VI Photoexposed and Photoprotected Human Skin: The Dominant Role of DHI." *Pigment Cell Res* 14 (2001): 337–347.
- Amelink A, Sterenborg H, Bard M, Burgers S. "In vivo measurement of the local optical properties of tissue by use of differential path-length spectroscopy." *Opt. Lett.* 29 (2004): 1087-1089.
- Coleman T, Li Y. "An Interior Trust Region Approach for Nonlinear Minimization Subject to Bounds." *SIAM Journal on Optimization* 6 (1996): 418-445.
- Coleman T, Li Y. "On the Convergence of Reflective Newton Methods for Large-Scale Nonlinear Minimization Subject to Bounds." *Mathematical Programming* 67 (1994): 189-224.
- Costin GE, Hearing VJ. "Human skin pigmentation: Melanocytes modulate skin color in response to stress." *FASEB J* 21 (2007): 976-994.
- Fitzpatrick TB. "The validity and practicality of sunreactive skin type-I through type-VI." *Arch Dermatol* 124 (1988): 869–871.
- Flock S, Jacques S, Wilson B, Star W, van Gemert M. "Optical Properties of Intralipid: A phantom medium for light propagation studies." *Lasers in Surgery and Medicine* 2 (1992): 510-519.
- González FJ, Martínez-Escanamé M, Muñoz RI, Torres-Álvarez B, Moncada B. "Diffuse reflectance spectrophotometry for skin phototype determination." *Skin Research and Technology* 16 (2010): 397-400 .
- Jacques S. *Oregon Medical Laser Centre website*. 2001. <http://omlc.ogi.edu/spectra/melanin/index.html> (accessed November 24, 2011).
- Johns M, Giller CA, German DC, Liu H. "Determination of reduced scattering coefficient of biological tissue from a needle-like probe." *Optics Express* 13 (2005): 4828-4842.
- Karsten AE, Singh A, Braun MW. "Experimental verification and validation of a computer model for light–tissue interaction." *Lasers Med Sci* 27 (2012a): 79–86.
- Martelli F, Del Bianco S, Ismaelli A, Zaccanti G. *Light Propagation through Biological Tissue and Other Diffusive Media*. ISBN 978-0-8194-7658-6. SPI Press , 2010.
- Michielsen K, De Raedt H, Przeslawski J, Garcia N. "Computer simulation of time-resolved optical imaging of objects hidden in turbid media." *Physics Reports* 304 (1998): 89-144.
- Pfefer TJ, Matchette L S, Bennett CL, Gall JA, Wilke JN, Durkin AJ, Ediger M. "Reflectance-based determination of optical properties in highly attenuating tissue." *Journal of Biomedical Optics* 8 (2003): 206–215.
- Prahl S. *Oregon Medical Laser Centre website - Optical Absorption of Hemoglobin*. 1999. <http://omlc.ogi.edu/spectra/hemoglobin/index.html> (accessed November 24, 2011).
- Simpson R, Kohl M, Essenpreis M, Cope M. "Near-infrared optical properties of ex vivo human skin and subcutaneous tissues measured using the Monte Carlo inversion technique." *Phys. Med. Biol* 43 (1998(a)): 2465–2478.
- Star WM. "Light dosimetry in vivo." *Phys. Med. Biol.* 42 (1997): 763-787.
- Tseng S, Bargo P, Durkin A, Kollias N. "Chromophore concentrations, absorption and scattering properties of human skin in-vivo." *Optics Express* 17 (2009): 14599-14617.
- Tuchin V. *Tissue Optics: Light Scattering Methods and Instruments for Medical Diagnostics*. 2nd edition, p 165-175. SPIE Press, 2007.
- van Staveren HJ, Moes CJM, van Marie J, Prahl SA, van Gemert MJC. "Light scattering in Intralipid-10% in the wavelength range of 400-1 1 00 nm." *Applied Optics* 31 (1991): 4507-4514.
- Zonios G, Bassukas I, Dimou A. "Comparative evaluation of two simple diffuse reflectance models for biological tissue applications." *Applied Optics* 47 (2008a): 4965-4973.
- Zonios G, Bykowski J, Kollias N. "Skin melanin, haemoglobin, and light scattering properties can be quantitatively assessed in vivo using diffuse reflectance spectroscopy." *J. Invest. Dermatol* 117 (2001): 1452-1457.
- Zonios G, Dimou A. "Modeling diffuse reflectance from semi-infinite turbid media: application to the study of skin optical properties." *Optics Express* 14 (2006): 8661-8674.

### 4.3 CONTRIBUTION OF THE DIFFUSE REFLECTANCE PROBE CALIBRATION TO THE WORK

The principle of using the diffuse reflectance probe measurements to calculate the absorption coefficient of skin has been established in the work described so far in this chapter. The initial measurements led to the notion that the contribution of eumelanin and pheomelanin should be separated in the data extraction algorithm. This was a new insight that was not explicitly found in the literature.

The next step was to implement the diffuse reflectance probe measurement system to determine the absorption coefficients for various South African skin phototypes. This work is described in the next section.

### 4.4 *IN VIVO* TESTS

In order to determine the extent of the absorption coefficient variation to be encountered in the South African population, a diverse group of 30 volunteers were recruited from the NLC staff for *in vivo* measurements with the diffuse reflectance probe. Due to the voluntary nature of the recruitment, the clinical study did not include individuals with skin phototype VI on the Fitzpatrick scale. In order to protect anonymity, only numbers were used to identify volunteers. For record purposes the outer part of the hand of each volunteer was placed next to a Fitzpatrick colour card to identify the skin phototype (see Figure 4.10, the same as Figure 2.5). This process has limited accuracy as there are only six colours/shades available to classify an individual's skin phototype, but at least provides some indication of the skin phototype. This was all that was required to do the initial data analysis.

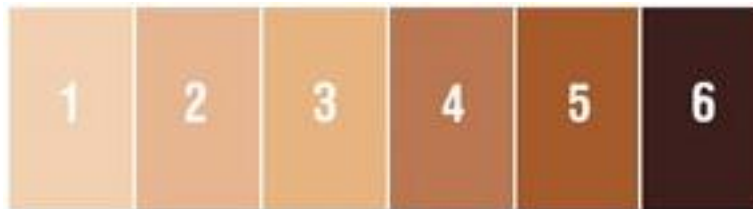


Figure 4.10: Fitzpatrick skin tone colour card.

As discussed in section 4.1, the results indicated the need to separate the contribution of melanin into the eumelanin and the pheomelanin. In literature there are a few hints to this effect, but to the knowledge of the author, it has not explicitly been used in the modelling work to extract the melanin concentrations. Two authors (Alaluf S, 2002(a)),

(Zonios G, 2006) indicated that there is a difference between the ratios of eumelanin and pheomelanin for individuals of different descent. In the later work of Zonios (Zonios G, 2008(c)) they favour a formulation that expresses the melanin extinction coefficient in terms of an exponential function with the decay governed by a parameter  $k_m$ . The value of  $k_m$  dictates the rate of the melanin extinction as function of wavelength. The shape of the extinction curves for different values of  $k_m$  do not provide an exact match for the published extinction curve data of eumelanin and pheomelanin. Being a parameter derived from the curve fit to the reflectance probe data, its purpose is to strike an amiable match between the distinct eumelanin and pheomelanin behaviour. Zonios (Zonios G, 2008(c)) has reported  $k_m$  values between 2 and 3 for skin phototype VI, which favours the more gradual extinction associated with predominantly eumelanin. For skin phototype III, they reported  $k_m$  values between 5 and 6.5, which accounts for the more rapid extinction associated with a greater presence of pheomelanin (Figure 4.11, the same as Figure 2.4 section 2.2.1.2).

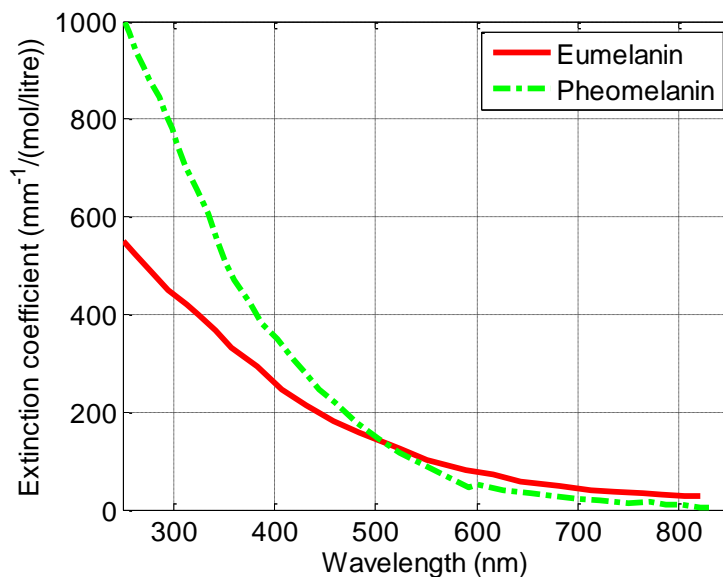


Figure 4.11: Absorption spectra of eumelanin and pheomelanin (data from (Jacques S, 2001)).

In a paper by Alulaf (Alulaf S, 2002(a)) it is stated:

“We observed a statistically significant trend (t-test;  $P < 0.05$ ), indicating that melanin composition becomes progressively more enriched with alkali soluble melanins as you move from the darkest (African) to the lightest (European) skin types. Similarly, a direct comparison of photoexposed and photoprotected skin within each ethnic group revealed (in most cases) a trend towards enrichment of alkali soluble melanins at photoprotected sites that was also consistent with previous observations, but was considerably smaller in magnitude than the variation in composition observed between different ethnic skin types.”

“As the relative contribution from different coloured melanin components varies in the skin, the colour of the final melanin pigment is likely to vary. Hence, skin may appear lighter, not only because it contains less melanin, but also because the melanin it contains is more lightly pigmented. Moreover, the manner in which this melanin is dispersed: either as single particles or as aggregated clusters may also affect how that final colour is perceived.”

Our results show that the ratio of eumelanin/pheomelanin concentrations for dark skin (phototype V) is 2.24 with a standard deviation of 1.82 and for the light skin phototypes I-III the ratio is 0.81 with a standard deviation of 0.30. Due to the limitations imposed by the ethical approval, the study could not include more volunteers in order to be able to statistically validate the data and compare the ratios. This is an area of research for the future.

Extracting the  $\mu_a$  values from the measured  $R_p$  spectra for the darker skin phototypes resulted in higher values than published in literature. Alaluf (Alaluf S, 2002(a)) reported eumelanin/pheomelanin concentration ratios for the sun-exposed ‘African skin’ (comparable to our phototype V skin) of 8.13 and 1.64 for the ‘European skin’ (comparable to our phototype I-II). Both ratios for Alaluf are about 3 times higher than our ratios. It should be noted that it is difficult to compare the results established by chemical extractions (used by Alaluf) with those of the integrated path optical method (used in this DRP work) in terms of the total absolute melanin ratios. At this point it may be important to note that the optical based values may be of more value for optical based treatments (laser based treatments) while chemical extraction may be more applicable to treatments based on pharmaceutical-chemical treatments.

Data presented in the paper below compares well with published data for the lower absorbance skin types (typically skin phototypes I-III). Our data indicated a difference in the  $\mu_a$  values for the skin areas exposed to sun and those that are not. This expected behaviour is also reported by Tseng (Tseng S, 2009) and Alaluf (Alaluf S, 2002(a)).

The depth of penetration for light in the diffuse reflectance measurements also has an effect on the calculated  $\mu_a$ . Meglinsky (Meglinsky IV, 2001) investigated the depth of measurement or measurement volume for different distances between the light source and the detector in diffuse reflectance systems. They concluded that a light source-detector spacing of 250  $\mu\text{m}$  primarily samples the epidermal layer and the papillary dermis. The light source-detector spacing in the probe used in this work was 200  $\mu\text{m}$ , indicating that the epidermal layer and the papillary dermis were sampled.

For the very light skin phototypes, the effect of the haemoglobin is visible in the  $R_p$  values (see Figure 4.12) through the local absorption peaks at 541 nm and 576 nm for

oxyhaemoglobin and 556 nm for deoxyhaemoglobin. This resulted in less accurate  $\mu_a$  values for the epidermis because the light also sampled the dermis (where the blood is present). The effect of such an error is not really significant in the application of this work. As reported later in Chapter 5, the effect of  $\mu_a$  between 0.001 and 0.05  $\text{mm}^{-1}$ , did not affect the light transmission values much. In the very dark skin phototypes (typically type V) in Figure 4.12, the effect of the haemoglobin is not visible in the  $R_p$  measurements. As such, the DRP is an applicable instrument to measure the absorption coefficient of the epidermis.

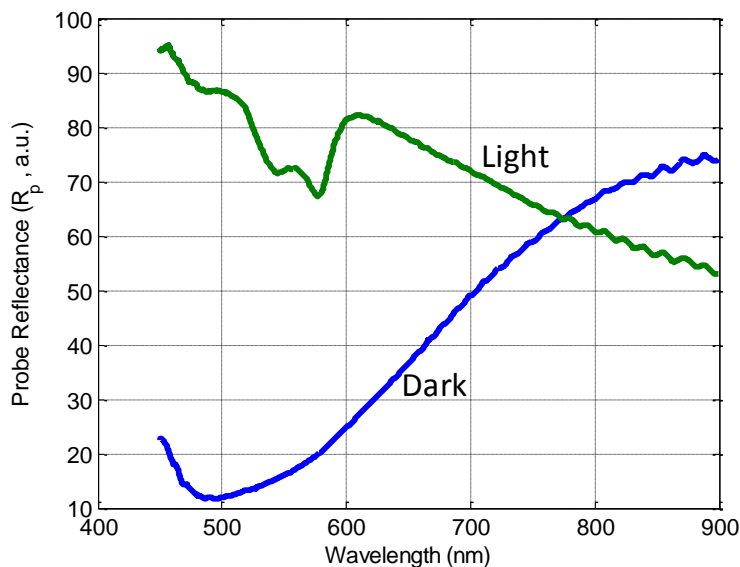


Figure 4.12: Reflectance measurements for two different skin phototypes.

More accurate methods may be available, but the diffuse reflectance probe offers a non-invasive, portable system with a quick turn-around time. It may be applicable in a clinical setting to quickly supply data that a health practitioner may use to establish optimal treatment parameters for an individual of any skin phototype.

#### 4.4.1 Paper on *in vivo* tests

The paper on the results of the *in vivo* study on the 30 volunteers was published online on 14 August 2012 in *Photochemistry and Photobiology* [doi: 10.1111/j.1751-1097.2012.01220.x].

Once again some minor alterations have been done to the published format of the paper to follow the style of the thesis.

## Diffuse reflectance spectroscopy as a tool to measure the absorption coefficient in skin: South African skin phototypes

A E Karsten<sup>1,2,\*</sup>, A Singh<sup>1</sup>, P A Karsten<sup>3</sup>, M W H Braun<sup>2</sup>

<sup>1</sup> Biophotonics Group, National Laser Centre, CSIR, P. O. Box 395, Pretoria, 0001, South Africa

<sup>2</sup> Department of Physics, University of Pretoria, Pretoria, 0002, South Africa

<sup>3</sup> Ballistics Research Group, Denel Land Systems, P O Box 7710, Pretoria, 0001, South Africa

\*Corresponding author's name and email: Aletta E Karsten (akarsten@csir.co.za)

### ABSTRACT

In any laser skin treatment, the optical properties (absorption and scattering coefficients) are important parameters. The melanin content of skin influences the absorption of light in the skin. The spread in the values of the absorption coefficients for the South African skin phototypes are not known. A diffuse reflectance probe consisting of a ring of six light delivery fibres and a central collecting fibre was used to measure the diffused reflected light from the arms of 30 volunteers with skin phototypes I-V (on the Fitzpatrick scale). The absorption coefficient was calculated from these measurements. This real time *in vivo* technique was used to determine the absorption coefficient of sun-exposed and sun-protected areas on the arm. The range of typical absorption coefficients for the South African skin phototypes is reported. The values for the darker South African skin types were much higher than was previously reported for darker skin phototypes. In the analysis the contributions of the eumelanin and pheomelanin were separated, which resulted in improved curve fitting for volunteers of southern Asian ethnicity without compromising the other groups.

### INTRODUCTION

Laser applications in both the medical and cosmetic industries have increased in recent years (Overton G, 2011). In many of these applications the laser light has to penetrate through some skin layers to reach the intended target site. Some laser treatments e.g. laser hair removal, rely on the penetration of the light through the outer skin layers to the root of the hair follicle. In the darker skin phototypes, light is absorbed in the outer skin layers and may cause burn wounds in the patient (Lanigan S, 2003). It is important that the treatment parameters are established accurately for each patient. The phototype of a patient's skin has been widely used to assist in the setting of these parameters.

At present, classifications of skin phototype or skin tone are mostly done according to the Fitzpatrick scale (Fitzpatrick TB, 1988). This subjective classification is based on the reaction of skin to sunlight (how easily an individual's skin will burn or change colour when exposed to sunlight or UV light) and is influenced by ethnicity and chronic sun exposure and cannot be used to determine the melanin content in skin (González FJ, 2010). This may not be sufficient for accurate and safe treatments (González FJ, 2010).

The epidermis contains basically three cell types: melanocytes, keratinocytes and Langerhans cells. Melanin is produced by the melanocytes. The diversity of the human skin phototypes is directly related to the melanin concentration in the epidermis. Melanin, located in the epidermal layer of the skin, consists of two major groups, eumelanin (black-brown colour) and pheomelanin (yellow-red colour). Darker skins do not necessarily have more melanocytes than lighter skins, but the melanocytes are more active (Störing M, 2004).

For laser related treatment both the laser wavelength and the melanin concentration in the epidermis have a major influence on the penetration depth of light and its absorption. In most applications direct, *in vivo*, measurements of the penetrated fluence rate are impractical. Computer simulations can be used to predict the fluence rate of laser light some distance into skin (Störing M, 2004), (Prahl S, 2007(a)), (Karsten AE, 2012(a)).

In order to use computer simulations, both the absorption coefficient ( $\mu_a$ ) and reduced scattering coefficient ( $\mu'_s$ ) of the skin must be known. Published data on the optical properties of skin are available but are

quite varied (Simpson R, 1998(a)), (Tuchin V, 2007) and are therefore difficult to apply to a specific individual. All the skin phototypes are present in the South African population, which poses an even greater challenge when laser treatment parameters from other parts of the world are applied locally.

Diffuse reflectance spectroscopy is a non-invasive *in vivo* measurement technique that has been used to estimate the optical properties ( $\mu_a$  and  $\mu'_s$ ) of skin (Johns M, 2005), (Zonios G, 2006). The technique takes very little time and can consequently be used to assess an individual just before treatment.

The work presented in this paper was done to establish whether (and to what extent) a diffuse reflectance probe can be used to determine the absorption coefficient of different skin phototypes, *in vivo*, in the South African population. A secondary objective was to establish the range of values of  $\mu_a$  and  $\mu'_s$  that reasonably represent the South African skin types.

In this work, the only source of difference between the respective volunteers was the melanin concentrations in the epidermal layer. Differences in the epidermal thickness were not explicitly taken into account, but formed part of the measurement. The effect of both the oxygenated and deoxygenated blood was also accounted for.

## MATERIALS AND METHODS

**Diffuse reflectance probe:** A diffuse reflectance probe (Ocean Optics R200-7-UV-VIS), a Halogen white light source (Ocean Optics HL-2000) and an Ocean Optics USB-4000 spectrometer, all from Ocean Optics Inc. (Florida, USA) were used in the experiments (Figure 4.13). The diffuse reflectance probe consists of seven 200  $\mu\text{m}$  optical fibres. The white light, emitting between 450 and 900 nm, was used for illumination and the spectrometer was used as a detector. The effective wavelength band for the system was from 450-800 nm.

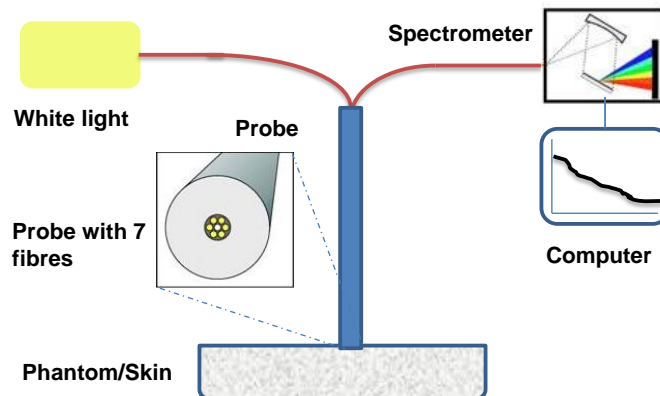


Figure 4.13: Experimental setup with the main system components (Karsten A, 2012(b)).

The Reflectance Wizard from the Ocean Optics Spectra Suite software was used in the measurements of the back reflected light. A calibration standard, WS-1 from Ocean Optics was used to calibrate the reflectance measurements. The back reflected light ( $R_p$ ) as a function of wavelength is given by:

$$R_p(\lambda) = -\log_{10} \left[ \frac{I_{meas}(\lambda) - I_D(\lambda)}{I_{ref}(\lambda) - I_D(\lambda)} \right] \quad (4.16)$$

where:

$I_{meas}(\lambda)$  = reflection spectrum

$I_D(\lambda)$  = detector dark current measurement

$I_{ref}(\lambda)$  = reflection spectrum obtained from the WS-1 calibration standard

The probe calibration procedure is described in an earlier paper (Karsten A, 2012(b)). The probe was calibrated on a set of liquid phantoms. The liquid phantoms were prepared from a mixture of 20% Intralipid (IL) (Sigma Aldrich, lot # 028K0740) and black ink (Trodar colour 7011). Calibration is required to map the geometrical parameters of the probe to the measured reflection data.

Diffuse reflectance can be expressed by an explicit dependence on  $\mu'_s$  and  $\mu_a$  (Zonios G, 2006). The diffused reflectance signal collected by the probe ( $R_p$ ) can be described by Eq. 4.17 (Zonios G, 2006):

$$R_p(\lambda) = \frac{\mu'_s(\lambda)}{k_1 + k_2\mu_a(\lambda)} \quad (4.17)$$

where  $k_1$  and  $k_2$  are calibration parameters that depend on the probe geometry and the experimental setup. These parameters were calculated from the phantoms as  $k_1 = 0.016312$  and  $k_2 = 0.019144$  (Karsten A, 2012(b)). Eq. 4.17 is based on the model described by Zonios (Zonios G, 2006) that assumes a single semi-infinite, homogeneous medium or layer. This simplified approach of the layered structure of the skin has been successfully used previously (Wu J, 1993), (Zonios G, 2006).

The major absorbing chromophores in human skin are haemoglobin, melanin water, carotene and bilirubin (Kollias N, 1995), (Dam JS, 2000(b)), (Meglinski IV, 2002), (Bashkatov AN, 2005). In the wavelength band 450-800 nm, used in this work, the effect of water absorption is at least an order of magnitude smaller than that of the haemoglobin and melanin (Dam JS, 2000(b)). The effect of the carotene and bilirubin was also excluded as parameters (Meglinski IV, 2002) in Eq 4.18 and Eq 4.19. The absorption coefficient ( $\mu_a$ ) can then be expressed in terms of the major absorbers, i.e. the blood (both oxyhaemoglobin and deoxyhaemoglobin) and melanin (Zonios G, 2006):

$$\mu_a(\lambda) = c_{Hb}[\alpha\varepsilon_{HbO_2}(\lambda) + (1 - \alpha)\varepsilon_{Hb}(\lambda)] + c_{mel}\varepsilon_{mel}(\lambda) \quad (4.18)$$

Due to unsatisfactory regression results to Eq. 4.17 with a single melanin parameter  $c_{mel}\varepsilon_{mel}(\lambda)$  for volunteers from southern Asian descent (with a yellow-red undertone), and the possibility that the ratio's between eumelanin and pheomelanin for individuals may vary (Alaluf S, 2002(a)), (Zonios G, 2006), the two different melanin types (eumelanin and pheomelanin) are accommodated explicitly (for all skin types) by rewriting Eq. 4.18 as:

$$\mu_a(\lambda) = c_{HbO_2}[\alpha\varepsilon_{HbO_2}(\lambda) + (1 - \alpha)\varepsilon_{Hb}(\lambda)] + c_{Eu}\varepsilon_{Eu}(\lambda) + c_{Pheo}\varepsilon_{Pheo}(\lambda) \quad (4.19)$$

The fibre optic probe introduces a linear dependence of the reflectance on the reduced scattering coefficient (Zonios G, 2006). The linear dependence of  $\mu'_s$  on wavelength (in the wavelength band 450 – 800 nm) has been justified by Zonios as a reasonable approximation which is supported by the Mie theory for spherical scatterers (Zonios G, 2001), (Zonios G, 2006), (Zonios G, 2008(b)). The reduced scattering coefficient ( $\mu'_s$ ) can be described by ((Zonios G, 2006)):

$$\mu'_s(\lambda) = \left[1 - c_d \left(\frac{\lambda - \lambda_1}{\lambda_2 - \lambda_1}\right)\right] \mu'_s(\lambda_{min}) \quad (4.20)$$

with:

- $\varepsilon_{HbO_2}(\lambda)$  = extinction coefficient for oxyhaemoglobin (Prahl S, 1999)
- $\varepsilon_{Hb}(\lambda)$  = extinction coefficient for deoxyhaemoglobin (Prahl S, 1999)
- $\varepsilon_{mel}(\lambda)$  = extinction coefficient for melanin (Jacques S, 2001)
- $\varepsilon_{Eu}(\lambda)$  = extinction coefficient for eumelanin (Jacques S, 2001)
- $\varepsilon_{Pheo}(\lambda)$  = extinction coefficient for pheomelanin (Jacques S, 2001)
- $c_d$  = parameter related to the effective light scatterer size in skin (Zonios G, 2001), (Zonios G, 2008(b))
- $c_{HbO_2}$  = oxyhaemoglobin concentration
- $c_{Hb}$  = deoxyhaemoglobin concentration
- $c_{mel}$  = melanin concentration
- $c_{Eu}$  = eumelanin concentration
- $c_{Pheo}$  = pheomelanin concentration
- $\alpha$  = oxygen saturation level of blood, defined as the percentage of the oxygenated blood of the total blood concentration  $\alpha = \frac{c_{HbO_2}}{c_{HbO_2} + c_{Hb}}$
- $\lambda_1$  = min ( $\lambda$ ) = 450 nm
- $\lambda_2$  = max ( $\lambda$ ) = 800 nm
- $\mu'_s(\lambda_{min})$  = ordinate of reduced scattering coefficient at  $\lambda_{min}$

The extinction coefficients are tabulated functions of wavelength (Prahl S, 2007(a)) and the associated concentrations are established through fitting procedures. The model assumes that all the chromophores contributing to the measurement are known in advance and that  $\mu'_s$  has a linear dependence on wavelength. This

is required to allow the separation of  $\mu_a$  and  $\mu'_s$  from the measured reflectance (Zonios G, 2006), (Tseng S, 2009). This technique can therefore not be used in a situation where unknown parameters need to be identified. At this stage the application of the technique is a non-invasive, real time, *in vivo* measurement to establish  $\mu_a$  for the skin of a specific individual. Fortunately the extinction coefficients for all the included chromophores are known (Tseng S, 2009).

The LSQCURVEFIT function from MATLAB was used to solve Eq. 4.17 through multiple linear regression. The measured probe reflectance is described mathematically in terms of 6 coefficients ( $c_{HbO_2}$ ,  $\alpha$ ,  $c_{Eu}$ ,  $c_{Pheo}$ ,  $c_d$ ,  $\mu'_s(\lambda_{min})$ ) that are adjusted to best match the equations to the experimental data. This simplistic technique was utilised with satisfactory effect by Zonios (Zonios G, 2006) and Marchesini (Marchesini R, 2009). The more complex alternative is a Monte Carlo simulation process as used by Meglinsky (Meglinsky IV, 2001), Johns (Johns M, 2005) and Reif (Reif R, 2007).

**Clinical data:** Volunteers were recruited at the National Laser Centre (NLC) and measurements were performed according to approved ethics proposals (CSIR: Ref 17/2011 and University of Pretoria: EC110830-060).

Measurements were done on the right arm of volunteers at two positions, one location was on the lower outer arm (sun exposed) and the other on the upper inner arm (not usually exposed to sun). These two positions were used in order to evaluate the inter-person difference due to the sun exposure on the melanin production and therefore skin tones. Ages of the volunteers ranged from 21 to 69 years and the group of 30 volunteers consisted of 11 females and 19 males. Skin phototypes of the volunteers were evaluated with a colour chart according to the Fitzpatrick scale and ranged from skin phototype I-V.

All the diffused reflectance measurements were done on the same day with the same reflectance standard calibration. The output of the halogen light source was monitored for 6 hours and over that period the fluctuations were less than 2.2 %, resulting in a very stable output.

Three measurements were done at each measurement position while the probe was kept in light contact with the skin surface. For each measurement the integration time for the probe was 20 ms and the signal was averaged 4 times, resulting in a total measurement time of 80 ms per measurement. Between volunteers, the probe was wiped clean with ethanol (99.9% from Promark Chemicals) for hygienic reasons and to remove any dirt/oiliness that may have been present on the probe.

## RESULTS

The results of reflectance probe ( $R_p$ ) measurements performed on the 30 volunteers are shown in Figure 4.14. In order to simplify the graph, the average spectrum of the three measurements per position for each individual was used except in a few cases where two of the spectra were close together and one was substantially distinct, most probably due to movement of the volunteer, which resulted in a sub-optimal measurement. From Figure 4.14 it is clear that the reflectance profiles for the different skin phototypes can be roughly categorised into three groups with respect to the overall trends in the graphs.

The trend for group A (typically of Caucasian descent) starts with a high  $R_p$  value and then decreases steadily, but with the effect of oxyhaemoglobin (local absorption peaks at 541 nm and 576 nm) and deoxyhaemoglobin (local absorption peak at 556 nm) manifesting between 540 nm and 580 nm. For group B (typically people from Indian, Asian and some African descent with a yellowish skin undertone) the absorption in the epidermis is higher and therefore the measurements start with a lower  $R_p$  value. The increased melanin concentrations mask the features associated with the haemoglobin. All group B measurements exhibit a generally horizontal trend as a function of wavelength.  $R_p$  values for group C (typical of African descent), begin much lower with an initial decrease up to around 500 nm and then show a steady increase in the reflectance value. In the third group the effect of the blood absorbance peaks is not visible in the reflectance graphs at this scale. This agrees with the expected general trend that higher absorbance skin types (higher melanin concentrations) will exhibit reduced diffuse reflectance due the increased melanin absorbance.

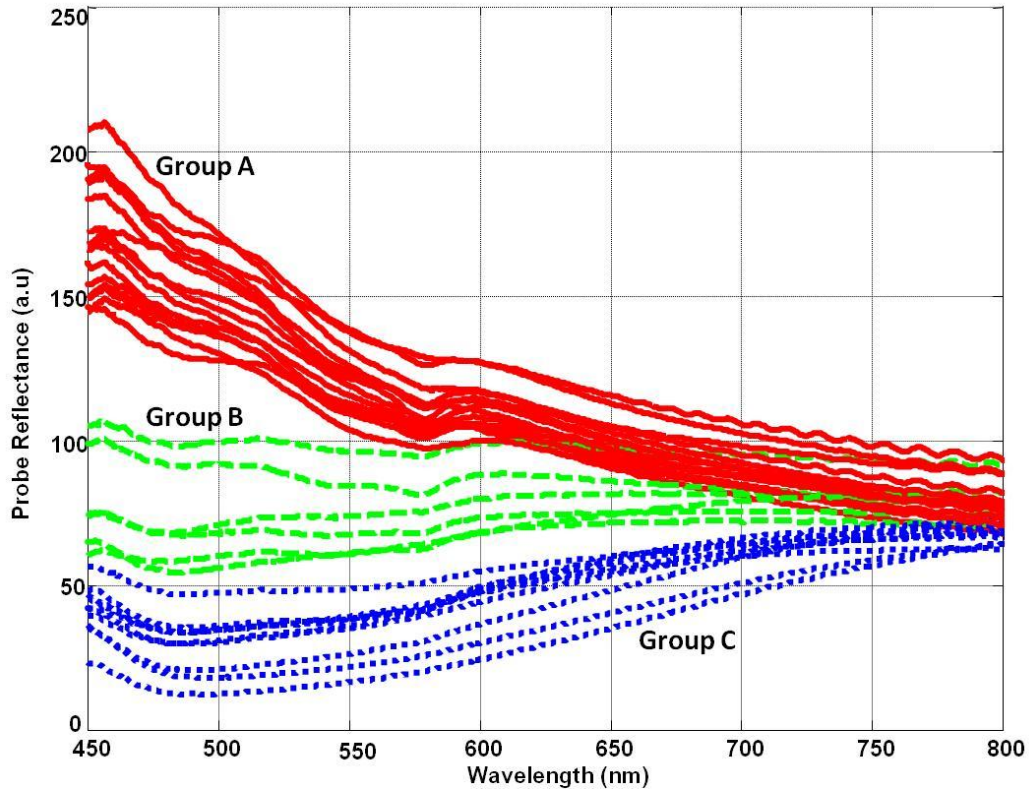


Figure 4.14: Reflectance probe measurements on the inner arm as a function of wavelength for all volunteers. Line styles were used to group graphs with similar trends.

Data analysis was then performed on all the measurements. For clarity in the graphical presentations the data was classified into two groups according to skin phototypes I-III and IV-V respectively. For one of the datasets, 29, the measurements were too scattered to be considered reliable and is not presented. Datasets 3 and 11 are also not presented because they gave unexpectedly high absorption values and the trend was quite different from the rest of the measurements. This ‘abnormality’ will require extensive further investigation before it may be considered as representative.

In Figure 4.15, the absorption coefficients (as calculated at a wavelength of 633 nm) are presented as bar graphs with the sun-exposed (outer arm) and non-exposed (inner arm) data for each volunteer. The lower absorbance skin types were grouped together in Figure 4.15(a) and the higher absorbance skin types were grouped together in Figure 4.15(b). One dataset, a skin phototype II, had a high value for the sun-exposed part of the arm ( $\mu_a = 0.084 \text{ mm}^{-1}$  for the outer arm). This result may be attributed to chronic sun exposure (permission to mention this fact was obtained from the volunteer concerned). This value is not shown in Figure 4.15(a), due to the influence on the  $\mu_a$  scale in the graph. Due to the spread in the  $\mu_a$  values some of the smaller values are not visible in Figure 4.15(b).

This first set of measurements is sufficiently accurate to set the ranges for absorption values for modelling purposes. In order to use the method on a routine basis before treatment, one must await standardised protocols over a range of many individuals of the skin types populations present in diverse.

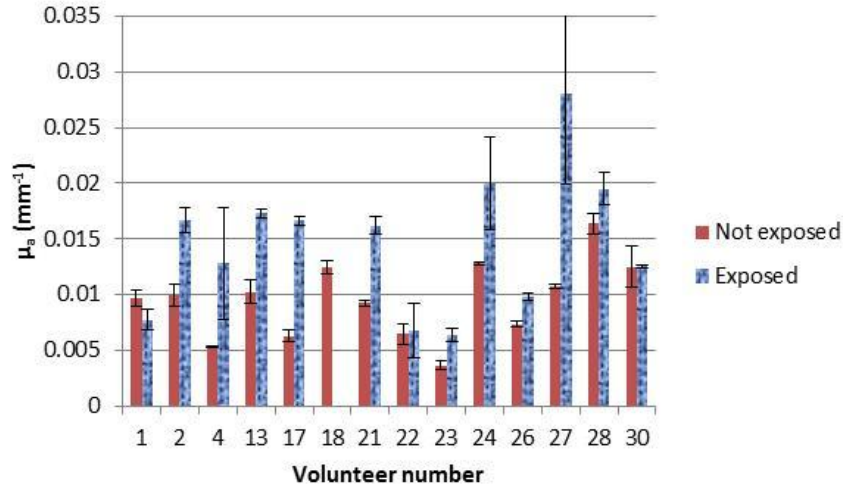


Figure 4.15(a): Absorption coefficients ( $\text{mm}^{-1}$ ) as calculated at a wavelength of 633 nm, for volunteers of skin phototypes I-III. The volunteer numbers are displayed on the X-axis. Sun-exposed value ( $0.084 \text{ mm}^{-1}$ ) for volunteer 18 is excluded from the graph for scaling purposes.

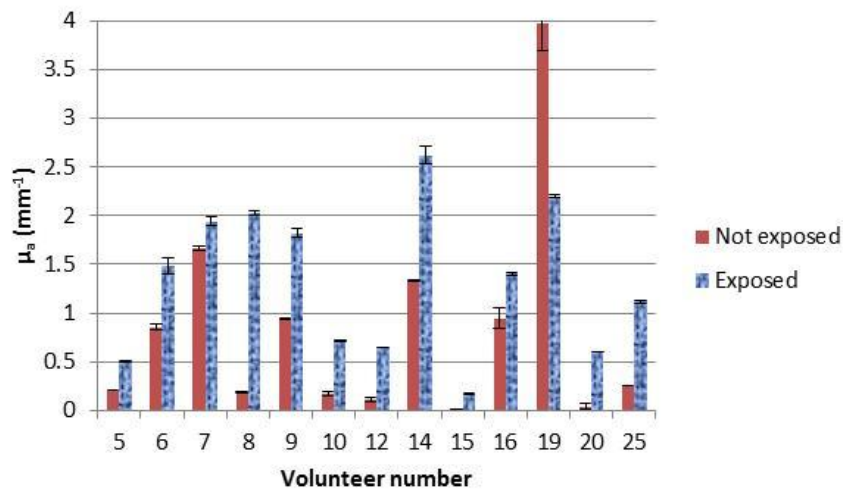


Figure 4.15(b): Absorption coefficients ( $\text{mm}^{-1}$ ) as calculated at a wavelength of 633 nm, for volunteers of skin phototypes IV-V. The volunteer numbers are displayed on the X-axis. The not exposed value ( $0.0075 \text{ mm}^{-1}$ ) for volunteer 15 is barely visible.

As a rule, the data shows the expected trend that the absorption coefficient is larger on the sun-exposed site than on the non-exposed site. For the lower absorbance skin types this assumption fails for only one person (volunteer 1). For the higher absorbance skin types (Figure 4.15(b)) there is only one exception to the generally expected behaviour that falls outside the experimental errors (volunteer 19). The reason for this is not clear at present, but there are two likely explanations. Shininess of the skin due to the use of moisturising creams (normally only applied to hands and lower arms – the measurement sites were not prepared or specifically cleaned before the measurements) is a possible reason. The use of moisturising creams was overlooked as a question in the questionnaire and was therefore not an exclusion criterion. Moisturising creams are normally applied to the hands and lower arm, resulting in a higher reflection from the skin and therefore a reduced ‘perceived’ absorbance. This was subsequently confirmed with measurements before and after applying petroleum based cream to the outer arm of a volunteer. The second possibility is sub-optimal probe contact with the skin of the upper arm which would typically result in lower  $R_p$  measurements.

In Figure 4.16 the absorption coefficient as a function of wavelength is given for the outer arm measurements on (Figure 4.16(a)) the lower absorbance skin group and (Figure 4.16(b)) the higher absorbance skin group.

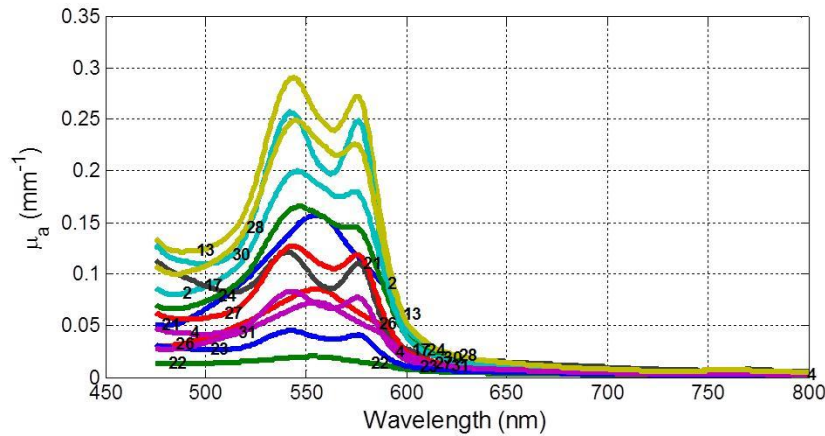


Figure 4.16 (a): Absorption coefficient as a function of wavelength for the lower absorbance volunteers. Measurements were done on the outer arm (sun-exposed).

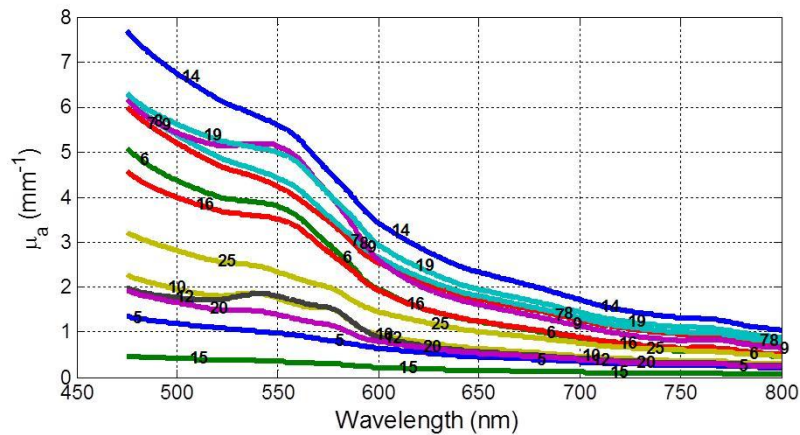


Figure 4.16(b): Absorption coefficient as a function of wavelength for the higher absorbance volunteers. Measurements were done on the outer arm (sun-exposed).

The results in Figure 4.16(a), clearly show the effect of the oxyhaemoglobin (double absorption peaks at wavelengths 511 nm and 576 nm) and deoxyhaemoglobin (single absorption peak at wavelength 556 nm) on  $\mu_a$ . This effect is not as clear in the higher absorbance skin types (Figure 4.16(b)). This is most likely attributable to the greater absorbing effect of increased melanin in the epidermis that obscures the haemoglobin absorption. The data in Figure 4.16(b) mimics the general trend of the melanin extinction coefficient, a decrease as a function of increasing wavelength. Most laser treatments that need to penetrate the skin use longer wavelengths (> 600 nm) in order to limit the effect of haemoglobin absorption.

This study was conducted to extract the typical range for  $\mu_a$  for a sample of the South African population. In Table 4.7, the minimum and maximum  $\mu_a$  and  $\mu'_s$  values for three wavelengths are listed. These wavelengths were selected due to the relevance for typical laser treatment wavelengths.

Table 4.7: Minimum and maximum  $\mu_a$  and  $\mu'_s$  values at wavelengths, 561, 633 and 676 nm.

$\lambda$ (nm)	Skin phototype I-III				Skin phototype IV-V			
	$\mu_a(\min)$ (mm <sup>-1</sup> )	$\mu_a(\max)$ (mm <sup>-1</sup> )	$\mu'_s(\min)$ (mm <sup>-1</sup> )	$\mu'_s(\max)$ (mm <sup>-1</sup> )	$\mu_a(\min)$ (mm <sup>-1</sup> )	$\mu_a(\max)$ (mm <sup>-1</sup> )	$\mu'_s(\min)$ (mm <sup>-1</sup> )	$\mu'_s(\max)$ (mm <sup>-1</sup> )
561	0.019	0.140	1.072	2.218	0.045	7.491	1.188	3.521
633	0.004	0.028	0.996	1.874	0.009	3.939	1.187	3.424
676	0.003	0.021	0.951	1.667	0.007	3.090	1.186	3.366

The eumelanin/pheomelanin ratio is also important to note. The results of this study showed that for the darkest skins (Phototype V) the sun-exposed eumelanin/pheomelanin ratio is 3.12 with a standard deviation of 1.85 and for the lighter skin phototypes I-III the ratio is 0.64 with a standard deviation of 0.58. At present this is just an indication of the variance in the ratio and to establish statistically reliable results, a study should be done on a much larger population.

## DISCUSSION

The results in this paper indicate that a diffuse reflectance probe can be used non-invasively on an individual basis to establish optical properties ( $\mu_a$  and  $\mu'_s$ ) of skin for the purpose of determining optimal and safe treatment parameters for Fitzpatrick skin types I-IV. For the skin type V the procedure results in higher than expected  $\mu_a$  values for some individuals. Treatment regimens can be optimised for all skin types by adjusting the laser intensity, the exposure time and the number of treatments.

In the sampling done for this work, there were no volunteers of skin phototype VI. Most indigenous South Africans are classified between I and V on the Fitzpatrick scale and as such the sample represented the range of South African skin phototypes.

Upper and lower limits of  $\mu_a$  for skin in the general South African population (see Table 4.7) were established. In Table 4.8 some of the comparable published data are presented. Very few results are available for higher absorbance skin types.

Table 4.8: Absorption coefficients from literature using similar diffuse reflectance techniques (Reflectance) as well as an integrating sphere (IS).

Method	$\mu_a$ (mm <sup>-1</sup> )	Position	Skin phototype	$\lambda$ (nm)	Ref
Reflectance <i>in vivo</i>	0.017±0.001	Outer Forearm	-	633	(Doornbos R, 1999)
Reflectance <i>in vivo</i>	0.0128±0.0005	Outer Forearm	-	660	(Doornbos R, 1999)
Reflectance <i>in vivo</i>	0.009±0.0002	Outer Forearm	-	700	(Doornbos R, 1999)
IS <i>ex vivo</i>	0.035	Abdominal and breast	Caucasian	633	(Simpson R, 1998(a))
IS <i>ex vivo</i>	0.022	Abdominal and breast	Caucasian	676	(Simpson R, 1998(a))
IS <i>ex vivo</i>	0.25	Abdominal and breast	Negroid	633	(Simpson R, 1998(a))
IS <i>ex vivo</i>	0.18	Abdominal and breast	Negroid	676	(Simpson R, 1998(a))
Reflectance <i>in vivo</i>	0.060	Inner upper arm	I-II	633	(Tseng S, 2009)
Reflectance <i>in vivo</i>	0.0616	Inner upper arm	III-IV	633	(Tseng S, 2009)
Reflectance <i>in vivo</i>	0.0705	Inner upper arm	V-VI	633	(Tseng S, 2009)
Reflectance <i>in vivo</i>	0.063	Outer Forearm	I-II	633	(Tseng S, 2009)
Reflectance <i>in vivo</i>	0.066	Outer Forearm	III-IV	633	(Tseng S, 2009)
Reflectance <i>in vivo</i>	0.073	Outer Forearm	V-VI	633	(Tseng S, 2009)
IS post mortem	0.069±0.013	-	Caucasian	600	(Tuchin V, 2007)

Data presented in this paper compares well with published data for the lower absorbance skin types. Our data indicated a difference in the  $\mu_a$  values for the skin areas exposed to sun and those that are not. This expected behaviour is also reported by Tseng (Tseng S, 2009) and Alaluf (Alaluf S, 2002(a)). When reporting on the measured data in this paper, the data was not grouped together according to the Fitzpatrick skin phototypes and averages reported, as is often done. When a patient is treated with a laser, the best treatment parameters would be those measured and calculated on the patient at the treatment site and not the skin type obtained by visual comparison with a colour chart that follows the Fitzpatrick scale. In this work an optical characterization method was used to identify the absorption coefficient that can be used in planning for optical treatments.

Our measurements for the higher absorbance skins differ from previously reported data (Table 4.8). The reason for this is not clear at present. Tseng (Tseng S, 2009) reported much smaller  $\mu_a$  values than one would expect (see Table 4.8). Alaluf (Alaluf S, 2002(a)) reported on melanin concentration for the different skin phototypes (typically South African). Their findings were that the 'African' skin had about double the melanin

concentration of the ‘European’ skin in the epidermis. This was true for both the sun exposed and not sun-exposed skin samples retrieved from 4 mm punch biopsies. Our results showed significantly higher differences in the absorption coefficient between lower and higher absorbance skin types.

The method used in this work measures the integrated optical effect of the different scatterers and absorbers (chromophores) present in skin. This is an optical measurement as opposed to a chemical analysis process where the melanin is extracted from the skin biopsy samples and the concentrations reported. When calibrations were done on skin simulating phantoms, the absorber was a single component, black ink. In this case there was a linear relation between the ink concentration and  $\mu_a$ . In skin it seems that the relation between the melanin concentration and  $\mu_a$  is not linear. It has been reported that the melanin particle sizes differ for skin types and are generally larger for the darker skin types (Tseng S, 2009). Tseng (Tseng S, 2009) has reported the possibility of crosstalk between  $\mu_a$  and  $\mu'_s$ , which may be due to melanin particles being partially scatterers as well as primarily absorbers. This potential crosstalk needs further investigation.

The skin was treated as an equivalent single layer bulk tissue and not as separate layers. As such the optical properties extracted for the measurements are average values over the different skin layers. The assumption of a mono layer is an oversimplification, but due to the small distance between the light delivery and light collection fibres, the probe only samples the epidermis and the dermis (Meglinski IV, 2002), (Zonios G, 2006). The fixed probe geometry used (six light delivery fibres surrounding a single collection fibre) does not allow for adjustment of measurements depths. The probe was calibrated on a single layer phantom and the calibration constants also took the geometry of the experimental setup into account. The main aim of this work was to measure the absorption coefficient of different skin phototypes non-invasively.

In most laser applications for skin treatment (both medical and cosmetic), the laser light penetrates some distance into the skin for the effective treatment. In such applications it is important that the absorption due to the melanin in the epidermis is understood in order to prevent damage, e.g. skin burning, as has been reported during laser hair removal for higher absorbance skin types (Lanigan S, 2003), (Battle E, 2004).

Regarding the depth of measurements of the probe, Meglinsky (Meglinski IV, 2002) investigated the depth of measurement or measurement volume for different distances between the light source and the detector in diffuse reflectance measurements. They concluded that a light source-detector spacing of 250  $\mu\text{m}$  primarily samples the epidermal layer and the papillary dermis. The light source-detector spacing in the probe used in this work was 200  $\mu\text{m}$ , indicating that the epidermal layer and the papillary dermis were sampled.

The data extraction in this paper separated the contribution of eumelanin and pheomelanin and this appeared necessary to allow the inclusion of people of southern Asian ethnicity. The average sun-exposed eumelanin/pheomelanin ratio for the darkest skins (Phototype V) calculated from our results is 3.12 and for the lighter skin (Phototypes I-III) the ratio is 0.64. Alaluf (Alaluf S, 2002(a)) reported eumelanin/pheomelanin ratios for the sun-exposed ‘African skin’ (comparable to our Phototype V skin) of 8.13 and 1.64 for the ‘European skin’ (comparable to our Phototype I-II). Both ratios for Alaluf are around 2.5 times higher than our ratios. Alaluf used 4 mm punch skin biopsies from 48 volunteers on both sun-exposed and non-exposed sites (three to four biopsies per site). Chemical analysis was used to extract the different melanin components through a process described in (Alaluf S, 2002(a)). It should be noted that it is difficult to compare the results established by chemical extractions with those of the integrated path optical method in terms of the total absolute melanin ratios.

The results of this pilot study showed that the diffuse reflectance probe has the potential to be used as a fast, non-invasive absorption measurement technique just before laser treatment. The absorption coefficient values obtained through this method can be implemented in software that models the light propagation through skin. In order to apply the technique with confidence in a clinical setting, the technique still needs to be verified with diffuse reflectance probe measurements on a much larger sample of the population. In future studies, experimental procedure should include the preparation of the measurement site by cleansing with an alcohol swab to ensure the best possible consistency of the skin surface.

## Acknowledgements

The authors would like to acknowledge Mr Bafana Moya for his work in the laboratories.

## REFERENCES

- Alaluf S, Atkins D, Barrett K, Blount M, Carter N, Heath A. "Ethnic Variation in Melanin Content and Composition in Photoexposed and Photoprotected Human Skin." *Pigment Cell Res* 15 (2002a): 112-118.
- Bashkatov AN, Genina EA, Kochubey VI, Tuchin VV. "Optical properties of human skin, subcutaneous and mucous tissues in the wavelength range from 400 to 2000 nm." *J. Phys. D: Appl. Phys.* 38 (2005): 2543-2555.
- Battle E, Hobbs L. "Laser-assisted hair removal for darker skin types." *Dermatologic Therapy* 17 (2004): 177-183.
- Dam JS. *Optical analysis of biological media - continuous wave techniques*. ISBN 91-628-4546-2. Lund Reports on Atomic Physics LRAP-265, 2000.
- Doornbos R, Lang R, Aalders M, Cross F, Sterenborg H. "The determination of in vivo human tissue optical properties and absolute chromophore concentrations using spatially resolved steady-state diffuse reflectance spectroscopy." *Phys. Med. Biol* 44 (1999): 967-981.
- Fitzpatrick TB. "The validity and practicality of sunreactive skin type-I through type-VI." *Arch Dermatol* 124 (1988): 869-871.
- González FJ, Martínez-Escanamé M, Muñoz RI, Torres-Álvarez B, Moncada B. "Diffuse reflectance spectrophotometry for skin phototype determination." *Skin Research and Technology* 16 (2010): 397-400.
- Jacques S. *Oregon Medical Laser Centre website*. 2001. <http://omlc.ogi.edu/spectra/melanin/index.html> (accessed November 24, 2011).
- Johns M, Giller CA, German DC, Liu H. "Determination of reduced scattering coefficient of biological tissue from a needle-like probe." *Optics Express* 13 (2005): 4828-4842.
- Karsten A, Singh A, Karsten P, Braun M. "Diffuse reflectance spectroscopy as a tool to measure the absorption coefficient in skin: system calibration." *Lasers in Medical Science* DOI 10.1007/s10103-012-1079-2 (2012(b)).
- Karsten AE, Singh A, Braun MW. "Experimental verification and validation of a computer model for light-tissue interaction." *Lasers Med Sci* 27 (2012a): 79-86.
- Kollias N. "The Physical Basis of Skin Color and its Evaluation." *Clinics in Dermatology* 13 (1995): 361-367.
- Lanigan S. "Incidence of side effects after laser hair removal." *J Am Acad Dermatol* 49 (2003): 882-886.
- Marchesini R, Bono A, Carrara M. "In vivo characterization of melanin in melanocytic lesions: spectroscopic study on 1671 pigmented skin lesions." *Journal of Biomedical Optics* 14 (2009): 014027.
- Meglinski IV, Matcher SJ. "Quantitative assessment of skin layers absorption and skin reflectance spectra simulation in the visible and near-infrared spectral regions." *Physiol. Meas.* 23 (2002): 741-753.
- Overton G, Anderson S, Belforte D, Hausken T. "Annual review and forecast." *Laser Focus World* 47 (2011): 40-60.
- Prahl S, *Oregon Medical Laser Centre website - Optical Absorption of Hemoglobin*. 1999. <http://omlc.ogi.edu/spectra/hemoglobin/index.html> (accessed November 24, 2011).
- Prahl S, *Oregon Medical Laser Centre website*. 2007. <http://omlc.ogi.edu/software/> (accessed December 13, 2011).
- Reif R, A'Amar O, Bigio I. "Analytical model of light reflectance for extraction of the optical properties in small volumes of turbid media." *Applied Optics* 46 (2007): 7317-7328.
- Simpson R, Kohl M, Essenpreis M, Cope M. "Near-infrared optical properties of ex vivo human skin and subcutaneous tissues measured using the Monte Carlo inversion technique." *Phys. Med. Biol* 43 (1998(a)): 2465-2478.
- Störning M. *Computer vision and human skin colour*. Ph.D. dissertation, Aalborg University, Denmark, URL: <http://www.cvmt.dk/~mst>, 2004.
- Tseng S, Bargo P, Durkin A, Kollias N. "Chromophore concentrations, absorption and scattering properties of human skin in-vivo ." *Optics Express* 17 (2009): 14599-14617.
- Tuchin V. *Tissue Optics: Light Scattering Methods and Instruments for Medical Diagnostics*. 2nd edition, p 165-175. SPIE Press, 2007.

- Wu J, Partovi F, Field MS, Rava RP. "Diffuse reflectance from turbid media: an analytical model of photon migration." *Applied Optics* 32 (1993): 1115-1121.
- Zonios G, Bykowski J, Kollias N. "Skin melanin, haemoglobin, and light scattering properties can be quantitatively assessed in vivo using diffuse reflectance spectroscopy." *J. Invest. Dermatol* 117 (2001): 1452-1457.
- Zonios G, Dimou A. "Melanin optical properties provide evidence for chemical and structural disorder in vivo." *Optics Express* 16 (2008(b)): 8263-8268.
- Zonios G, Dimou A. "Modeling diffuse reflectance from semi-infinite turbid media: application to the study of skin optical properties." *Optics Express* 14 (2006): 8661-8674.

#### 4.5 VALUE OF THE DIFFUSE REFLECTANCE PROBE MEASUREMENTS

The usefulness of the optical properties extracted from the probe measurements lie in their use in the computer model as minimum and maximum values for the absorption coefficient. The model however has some limitations. One of the limitations is that the current probe system does not allow for measurements at different depths into the skin. The depth of measurement is dictated by the distance between the emitting and collecting fibres and to some extent the absorption coefficient.

Another limitation in the experimental procedure was that the measurement site was not specifically prepared before measurements. In future work the site must be cleaned before the measurements to ensure there is no 'unwanted' residue of skin treatment products that may influence the measurements.

The extracted absorption coefficients are average values over the depth of the measurements. In future work the design of a probe with more than one collecting fibre at different distances must be investigated to evaluate the absorption coefficient at different depths into the skin and resolve the contributions of various skin layers.

The effect of blood absorption is noticeable in most of the data and it does have an influence on the absorption coefficient at shorter wavelengths. At the wavelengths considered in this work (and for most laser therapeutic applications), the effect is not important. At the treatment wavelengths (typically  $> 650$  nm), the effect of the blood on the dermal absorption is negligible and therefore the absorption coefficient extracted can be attributed mainly to the epidermal absorption.

The measurements were done on a very small sample of the population. The technique still needs to be refined on a much larger sample of the South African population before the system may be used with confidence in a clinical setting. The aim of the measurements was to establish the upper and lower limits for the epidermal absorption coefficients to be used in the computer model and was adequate for this limited purpose.

In the next chapter the epidermal absorption coefficients calculated from the diffuse reflectance probe measurements are used in the computer model to predict the influence of epidermal absorption on the treatment times during laser treatment.